Powder Technology 467 (2026) 121514

Contents lists available at ScienceDirect

Powder Technology

journal homepage: www.journals.elsevier.com/powder-technology

# Experimental measurements in a model silo with eccentric hoppers

Adriano Pinilla, José María Fuentes, Francisco Ayuga, Eutiquio Gallego *

*BIPREE Research Group, Universidad Politécnica de Madrid, ETS Ingeniería Agronómica Alimentaria y de Biosistemas, Avda. Puerta de Hierro 2, 28040 Madrid, Spain*

## HIGHLIGHTS

- Hopper eccentricity causes asymmetry in pressure distribution and other parameters.
- Highest discharge normal pressures were measured at the wall farthest from the outlet.
- Eccentricity induced highest frictional forces on the wall farthest from the outlet.
- The gravity center of the bulk material moved towards the wall farthest from the outlet with eccentricity.
- Mass flow rate for the full-eccentric hopper was significantly higher.

## GRAPHICAL ABSTRACT

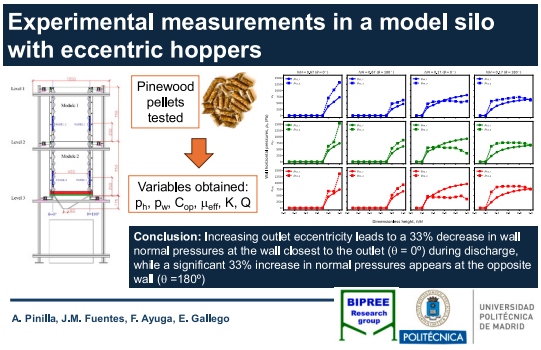


## ARTICLE INFO

*Keywords:*
Silo
Frictional forces
Lateral pressure ratio
Effective wall friction coefficient
Pinewood pellets
Corrugated walls

## ABSTRACT

This study analyses the effect of outlet eccentricity on wall pressures, frictional forces, effective wall friction coefficient, lateral pressure ratio and mass flow rate in a model silo made of corrugated steel and transparent polymethylmethacrylate walls. The silo model consists of two vertical modules (1.5 m in height and a 0.45 × 0.45 square cross section) and a hopper (0.175 m in height and a 0.06 × 0.06 m square outlet). Three different hoppers were used by varying the outlet eccentricity: centred (0 % eccentricity), half-eccentric (50 % eccentricity), and full-eccentric (100 % eccentricity). Pinewood pellets were used as the bulk solid material for the tests conducted. The results indicate that outlet eccentricity causes significant changes in pressure distributions and other parameters. An increase in normal pressure during the discharge was observed on the wall farthest from the outlet ($\theta = 180°$) compared to that measured at the end of the resting phase, while a progressive decrease appears at the wall closest to the outlet ($\theta = 0°$) when increasing hopper eccentricity. Outlet eccentricity also induces an increase of the frictional forces and the weight of the material resting over the hopper at the wall farthest from the outlet, with respect to the wall closest to the outlet. A similar pattern is observed for the lateral pressure ratio. A significantly higher mass flow rate was reported for the full-eccentric hopper with respect to the centred and half-eccentric hoppers.

* Corresponding author.
*E-mail address:* eutiquio.gallego@upm.es (E. Gallego).

https://doi.org/10.1016/j.powtec.2025.121514
Received 4 June 2025; Received in revised form 29 July 2025; Accepted 1 August 2025
Available online 5 August 2025

## 1. Introduction

Silos have been used to store all kind of granular materials in a wide range of facilities and industries. Many agricultural farms employ small steel silos that consist of a vertical bin and a hopper with outlet eccentricity (oblique hopper) that facilitates the flow of the material during the silo discharge. In addition, commercial steel silos usually have a sinusoidal corrugated wall since it allows a more efficient structural design [1]. The calculation of wall normal and tangential pressures on concentric conical hoppers is covered by the current European standard EN 1991–4 [2]. The equations included in Eurocode are attributed to Walker [3], despite they are based on the previous works by Dąbrowski [4]. However, the current version of EN 1991–4 does not cover oblique hoppers.

During the 20th century, a large number of experimental tests have been conducted to determine the pressures exerted by the stored material over bin walls [5 – 14]. However, very few research works refer to concentric hoppers [15 – 18], and only the tests implemented by Ramirez et al. considered oblique hoppers [19]. Aoki and Tsunakawa [15] measured wall normal pressures on steep hoppers, and they found a good agreement with the theoretical predictions of Walker for filling condition.

On the contrary, the wall normal pressures measured by Ding et al. [16] at the end of filling in a shallow concentric hopper were significantly higher than those predicted by Walker theory. This could be explained by the fact that shallow hoppers having large apex half angle does not fully mobilize wall friction, then leading to higher wall normal pressures. The results obtained by Ding et al. [16] were in a good agreement with the values predicted by Rotter theory for shallow hoppers [20], that essentially considers Walker theory with an effective hopper wall friction coefficient.

Ramirez et al. [19] measured wall normal pressures on bin-hopper full scale silos with smooth steel walls, and 3 different oblique hoppers with 0 %, 50 % and 100 % outlet eccentricities. They found a significant difference in wall normal pressures between the wall closest to the outlet and the opposite wall during discharge. Thus, larger wall normal pressures were reported for the wall location opposite to the hopper outlet for both materials tested (wheat and maize kernels). For experimental tests conducted with wheat, they found that the higher the outlet eccentricity, the higher wall normal pressures were found on the wall closest to the outlet at bin-hopper transition at the end of filling. This pattern was not so evident for maize, thus authors theorized that the inclination of the tube used for filling the silo could induce an eccentric filling that might cause the asymmetries in filling pressures.

Several researchers have proposed different analytical procedures to determine wall pressures on oblique hoppers [21 – 22], but assuming in such works a plane stress condition that is not applicable in real 3D silo hoppers. In addition, some Finite Element Models (FEM) have also been developed to study the possible effects of eccentricity on the filling pressures on oblique hoppers when compared to the concentric hopper [23 – 24]. The FEM models developed by Ayuga et al. [23] and Guaita et al. [24] predicted an increase in the wall normal pressures at the wall location opposite to the outlet, and a decrease in wall pressures in the wall closest to the outlet, when compared with a centric outlet. In addition, it was found for both walls that these differences increased with increasing outlet eccentricity. Vidal et al. [25 – 26] developed also a FEM model for bin-hopper silos with supporting elements, where they found that outlet eccentricity would affect the value of membrane and stress resultants between supporting columns. Gallego et al. [27] developed a FEM model that confirmed the findings of previous works and proposed an analytical equation to predict filling normal pressures on oblique hoppers that would consider parameters such as hopper aspect ratio, bin aspect ratio, outlet eccentricity, wall friction coefficient, wall circumferential location or the material stored in the silo. More recently, the Discrete Element Method (DEM) has also been used to study the effect of outlet eccentricity in a flat bottom silo [28 – 30]. The results obtained by these authors show that high asymmetric flow patterns are caused by outlet eccentricity, that also affects particle velocities.

At the same time, very few experimental tests have been conducted in silo walls with corrugated walls [31 – 33], despite there is evidence that the friction phenomena in these walls significantly differ from that existing in a smooth wall [34 – 37]. The friction phenomena produced by corrugated walls has been recently studied by several authors through DEM models [38 – 43].

The present work aims to study the effect of different outlet eccentricities of a hopper in wall normal pressures, frictional forces, effective wall friction coefficient or the mass flow rate. The tests have been conducted by employing a silo model supporting different bottom configurations [33]. These are the first experimental tests conducted in a bin-hopper silo configuration with corrugated walls and outlet eccentricity. The research tries to corroborate the findings of previous numerical works [24,27,29] with regards to the appearance of asymmetries in wall pressures or other parameters caused by the outlet eccentricity.

## 2. Material and methods

### 2.1. Description of the silo model

The experimental equipment used consisted of a model silo with a square cross-section of 0.45 × 0.45 $m^2$ and a total height of 1.5 m (Fig. 1). The vertical bin of the silo was composed of two independent modules, each 0.75 m high, supported by 4 beam-type load sensors located on levels 1 and 2 respectively, while the hopper or the flat bottom of the silo is supported by another 4 sensors located on level 3. All the sensors employed in the silo model were beam load cells provided by Hottinger Brüel & Kjaer GmbH (Darmstadt, Germany), either model K-SP4M-N-C3MR or HLCB1C3 (which have different maximum loads of 7, 20, 30, 50 and 550 kg depending on their location in the silo model). Their sensitivity is 2,0 ± 0,2 mV/V. An individual calibration for each sensor was made by the authors, and a linear response was obtained in the load measurement with errors <0.8 %. The data provided by the sensors were collected using a QuantumX MX1615 datalogger (HBK), at a sample rate of 100 Hz to capture the peak pressures typically occurring at the start of the silo emptying.

Several authors have observed scale effects in their work when measuring frictional stresses, deformations or flow of granular materials confined in moulds or scale silos, limiting the possibility of directly extrapolating the results obtained in small models to larger structures [44]. In this respect, the dimensions of the model silo used in this research are greater than 40 times the equivalent diameter of the granular particles to avoid the scale effect in the measurements of the grain-wall friction coefficients, as recommended by the European standard EN 1991–4.

The lateral walls of the silo were built with a commercial galvanised steel sheet with a sinusoidal profile with a wavelength of 75 mm and a corrugation height of 13 mm, fixed by means of countersunk screws to a 20 mm thick MDF wood board, to guarantee the structural rigidity of the wall and to avoid unwanted deformations. The front and back walls of the silo were made of transparent polymethylmethacrylate (PMMA) to allow visual monitoring of the material flow during unloading. On the corrugated walls, four square measuring panels with a cross-section of 0.15 × 0.15 $m^2$ equipped with sensors were mounted for the measurement of normal and tangential pressures.

Panels 1 and 2 were placed in the upper module at a height h = 1.0 m from the bin – hopper transition (relative height h/H = 0.67, where H refers to the total height of the silo bin), while panels 3 and 4 were placed in the lower module at a height h = 0.25 m from the bin - hopper transition (relative height h/H = 0.17). These distances refer to the centre of the corresponding test panel, which has been placed in the middle of the lateral walls. Furthermore, panels 2 and 4 are placed on

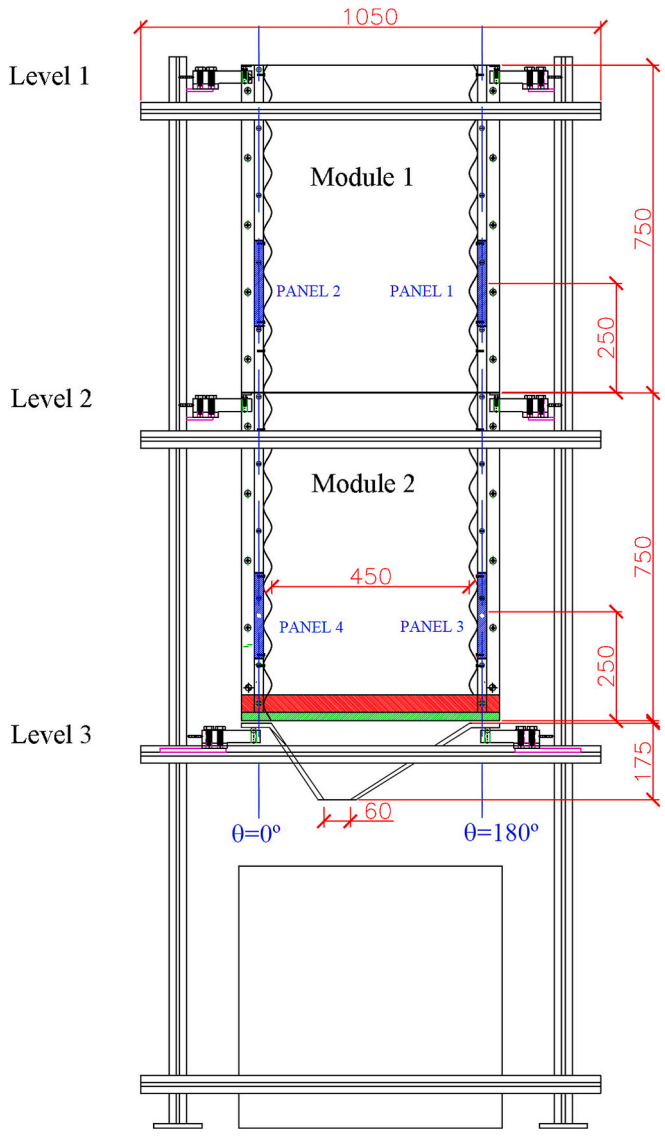


**Fig. 1.** Front view of the experimental silo (units in mm).

the wall adjacent to the outlet ($\theta = 0°$) and panels 1 and 3 on the opposite wall in the case of eccentric hopper discharge ($\theta = 180°$).

In this work, experimental tests were carried out using four different exchangeable bottom configurations, corresponding to: (i) flat bottom, (ii) centred hopper, (iii) hopper with 50 % eccentricity and hopper with 100 % eccentricity. The height of the hopper was 0.175 m for all cases and the dimensions of the outlet, which is square in cross-section, were in all cases 60 × 60 mm$^2$, regardless of the type of bottom used, with only the inclination of the hopper walls and the location of the outlet hole varying. Fig. 2 shows plan views of the different types of bottoms used in the research. The walls of the hoppers and the flat bottom were made of 3 mm thick steel plate to ensure structural rigidity and prevent possible deformations during the tests.

The silo filling process was carried out using buckets from the top of the silo, ensuring that the material fell centrally and at a constant rate (approx. 1.5 kg/s). Once filling was complete, the granular material was left to rest for 5 min before the outlet was opened to start discharging the material in free fall through the outlet of the different bottom configurations. The authors also checked that longer periods of time (up to 15 min) did not produce changes in the variables measured during the resting phase. Settling of material can appear for even longer periods of resting [45], but the changes in pressures would be minimum because of the reduced dimensions of the silo model implemented. A more detailed description of the silo model implemented can be found in [33].

The granular material used in the experimental tests were cylindrical pinewood pellets supplied by Nova Lenha Lda., with a diameter of 6 mm (± 0.1 mm) and a length varying between 4 and 32 mm. The physical and mechanical characteristics of the material, summarised in Table 1, were obtained by the authors using, among others, sieve analysis, bulk density measurements, direct shear tests, oedometric tests and triaxial tests [46 – 48].

Seven different replicates of the experiment were carried out for each selected background configuration to ensure the repeatability of the tests and to minimize possible errors due to experimental variations. The mean value, standard deviation (SD) and coefficient of variation (CV) were recorded for each variable measured. Shapiro-Wilk and Levene tests were used to confirm the normality and homoscedasticity of the results [49–51]. Differences between variables were sought by analysis of variance (ANOVA) followed by Tukey's test [52 – 53]. The significance level was set at $p < 0.05$.

**Table 1**
Main properties of the pinewood pellets used in the experimental tests.

| Variable | | Value |
|---|---|---|
| Dimensions | Length, L [mm] | 15.92 ± 5.98 |
| | Diameter, φ [mm] | 6.08 ± 0.05 |
| | Diameter of equivalent spherical particle, $\phi_{Eq.}$ [mm] | 9.36 ± 1.20 |
| Humidity [%] | | 6 |
| Density of wood pellet particles, $\rho_p$ [kg/m$^3$] | | 1227 ± 18.02 |
| Specific bulk weight, γ [kN/m$^3$] | | 6.5 |
| Angle of repose, $\varphi_r$ [°] | | 40.5 |
| Angle of internal friction, $\phi_i$ [°] | | 39.5 |
| Coefficient of friction with a smooth steel sheet, $\mu_w$ | | 0.3 |
| Effective wall friction coefficient according to EN 1991–4, $\mu_{eff,\ EN}$ | | 0.72 |

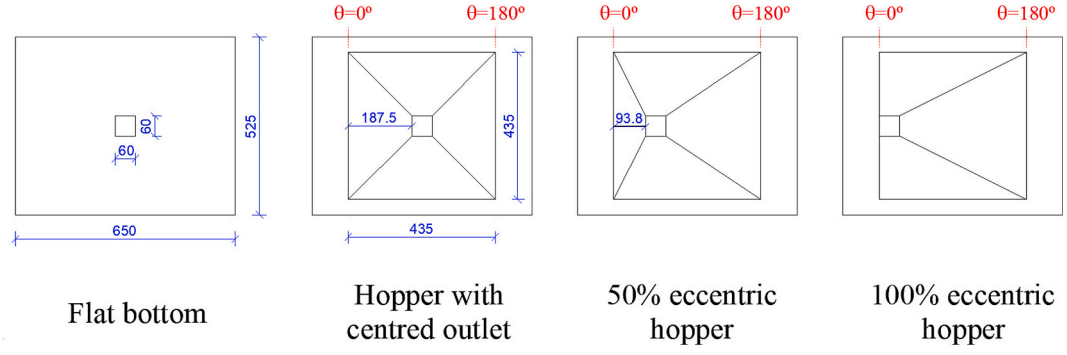


**Fig. 2.** Hopper configurations used in the experimental tests (units in mm).

### 2.2. Variables studied

The measurements provided by the different beam load cells employed in the silo model allow calculating different variables of interest for the analysis of the structural behaviour of the silo model, e.g. wall normal and tangential pressures or mass flow rate, among others. The description of the variables and measurements considered can be found in the notation list. The calculation of these variables usually requires employing the weight, mass, bulk density or height of the material stored in the silo, which can be obtained through Eqs. 1–4. The total weight, $W_t$, of the material stored in the silo for a specific instant of time (Eq. 1) can be calculated through the sum of the measurements $F_{Yij}$ provided by the twelve sensors placed at the 3 levels shown in Fig. 1, where i refers to the levels (3 levels) and j refers to the sensors located at one specific level (4 sensors in each level). Fig. 3 shows the direction of the different forces measured by the sensors.

The mass of the bulk solid stored at any instant, $M_t$, can be obtained by simply dividing the weight with gravity acceleration, g (Eq. 2). The bulk density of the material (Eq. 3) used in the calculations, γ, was obtained at the end of the resting phase, considering the total weight of the material stored inside the silo, W, the volume of the vertical section, $V_v$, and the volume of the hopper, $V_h$. Finally, it is important to state that the filling height of the material at any instant of time, $h_t$, is measured with respect to the bin–hopper transition (Eq. 4), and its calculation also requires to consider the mass stored at the hopper, $M_h$, and the area of the bin cross section, A. It has been assumed the existence of a constant value of the bulk density to calculate the mass stored at the hopper.

$$W_t = \sum_{i=1,3}^{j=1,4} F_{Yij} \tag{1}$$

$$M_t = \frac{\sum_{i=1,3}^{j=1,4} F_{Yij}}{g} \tag{2}$$

$$\gamma = \frac{W}{V} = \frac{M \bullet g}{V_v + V_h} = \frac{\sum_{i=1,3}^{j=1,4} F_{Yij}}{V_v + V_h} \tag{3}$$

$$h_t = \frac{M_t - M_h}{A \bullet \left(\gamma / g\right)} = \frac{\sum_{i=1,3}^{j=1,4} F_{Yij} - \gamma \bullet V_h}{A \bullet \gamma} \tag{4}$$

#### 2.2.1. Normal and tangential pressures on the test panels

The lateral and vertical forces measured at every test panel (Figure 3) are used to determine the normal (Eq. 5) and tangential (Eq. 6) pressures by dividing the corresponding force between the effective area of each test panel, $A_p$.

$$p_{hi} = \frac{F_{Xi}}{A_p} \tag{5}$$

$$p_{wi} = \frac{F_{Yi}}{A_p} \tag{6}$$

#### 2.2.2. Overpressure coefficients

The dynamic effects existing and the change in the stress state of the bulk material during the discharge phase usually leads to the existence of significant pressure increases for symmetric silos. Besides, the existence of eccentric hoppers can also significantly change the wall pressure distribution. Because of that, it has been calculated the ratio between the maximum pressure measured during discharge and filling for both the normal (Eq. 7) and tangential (Eq. 8) pressures. The overpressure coefficient for normal pressures, $C_{op,h}$, has been obtained as the ratio between the maximum pressure measured during discharge process, $p_{h,d}$, and the maximum pressure registered at the end of the resting phase, $p_{,fh}$. A similar procedure has been used to calculate the overpressure coefficient for tangential pressures, $C_{op,w}$, from the maximum values obtained during discharge, $p_{w,d}$, and at the end of the resting phase, $p_{w,f}$.

$$C_{op,h} = \frac{p_{h,d}^{max}}{p_{h,f}^{max}} \tag{7}$$

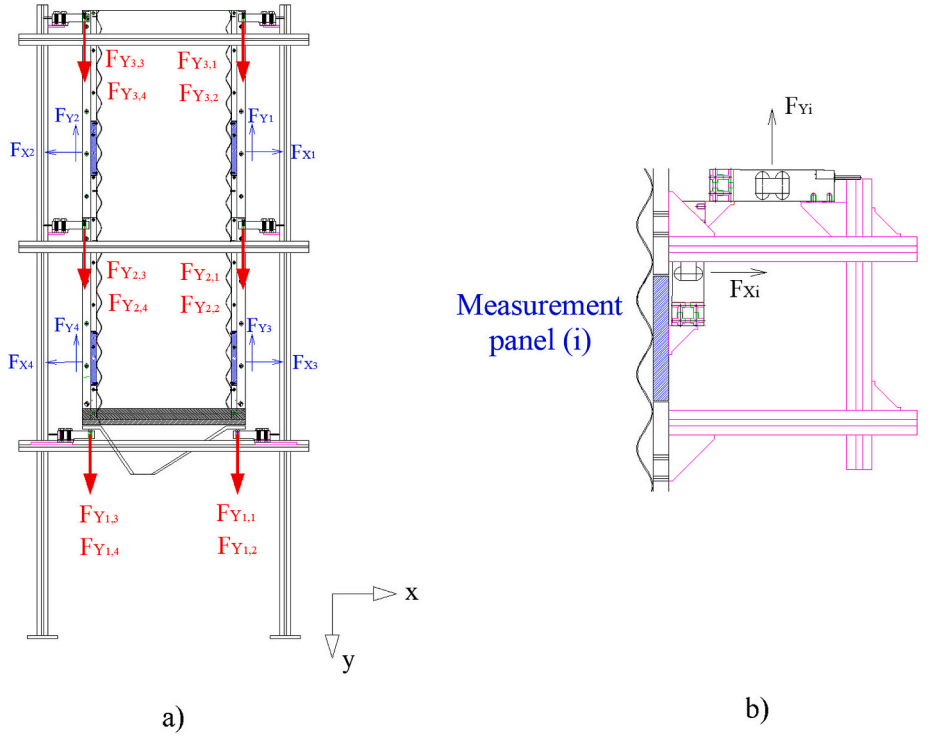


**Fig. 3.** a) Diagram of forces measured by the load cells installed in the model silo. b) Diagram of forces acting on the measurement panels 1 to 4.

$$C_{op,w} = \frac{p_{w,d}^{max}}{p_{w,f}^{max}} \quad (8)$$

#### 2.2.3. Effective wall friction coefficient

The experimental value of the effective wall friction coefficient existing on the corrugated wall is calculated at any test panel by dividing the measured tangential, $p_w$, and normal pressures, $p_h$, respectively (Eq. 9).

$$\mu_{eff,i} = \frac{p_{wi}}{p_{hi}} = \frac{F_{Yi}}{F_{Xi}} \quad (9)$$

Because of the existence of eccentric hoppers, it might be interesting to distinguish the total frictional forces measured at every vertical module in both walls (Eqs. 10–11). In this instance, the subscript "L" refers to the wall closest to the outlet ($\theta = 0°$), while the subscript "R" refers to the wall opposite to the outlet ($\theta = 180°$). Therefore, $F_{w1}$ refers to the total frictional forces measured at the upper vertical module, and it is calculated as the sum of the forces measured in the two sensors located at $\theta = 180°$ ($F_{w1R}$, which is the sum of $F_{Y11}$ and $F_{Y12}$) and the two sensors located at $\theta = 0°$ ($F_{w1L}$, which is the sum of $F_{Y13}$ and $F_{Y14}$). The total frictional forces measured at the lower vertical module, $F_{w2}$, have been obtained following a similar procedure.

$$F_{w1} = F_{w1R} + F_{w1L} = (F_{Y11} + F_{Y12}) + (F_{Y13} + F_{Y14}) = \sum_{j=1}^{4} F_{Y1j} \quad (10)$$

$$F_{w2} = F_{w2R} + F_{w2L} = (F_{Y21} + F_{Y22}) + (F_{Y23} + F_{Y24}) = \sum_{j=1}^{4} F_{Y2j} \quad (11)$$

It has also been obtained the theoretical value of the effective wall friction coefficient against a corrugated wall by employing the equation proposed by Eurocode EN 1991–4 (Eq. 12), where $\mu_w$ is the friction coefficient against an smooth wall, $\varphi_i$ is the angle of internal friction of the bulk material and $a_w$ is the wall contact factor. It is important to remark that EN 1991–4 suggests using $a_w = 0.2$ value for corrugated walls with sinusoidal profile.

$$\mu_{eff,EN} = (1 - a_w) \bullet \tan\varphi_i + a_w \bullet \mu_w \quad (12)$$

#### 2.2.4. Lateral pressure ratio

The lateral pressure ratio, K, is defined as the ratio between the normal pressure over the silo wall, $p_h$, and the vertical pressure, $p_v$, existing at a certain silo height. This coefficient was obtained at the location of test panels situated at $h/H = 0.17$ (Eq. 13) and $h/H = 0.67$ (Eq. 14).

$$K_i = \frac{p_{hi}}{p_{vt}} \ (i = 3 \text{ or } 4) \quad (13)$$

$$K_i = \frac{p_{hi}}{p_{vv}} \ (i = 1 \text{ or } 2) \quad (14)$$

The calculation of K for test panels located at $h/H = 0.17$ requires determining the vertical pressure existing at the bin–hopper transition, $p_{vt}$, that is obtained through Eq. 15, where $W_{vt}$ is the weight of the stored material resting over the silo bottom, $W_{vh}$ is the weight of the material stored in the hopper, and A refers to the area of the bin cross section. The value of $W_{vt}$ is obtained with the measurements provided by the sensors supporting the hopper at level 3 ($F_{Y3j}$). On the other hand, the vertical pressure existing between the two vertical modules, $p_{vv}$, is needed to calculate K for test panels at $h/H = 0.17$ (Eq. 16). Its value is obtained by dividing the weight of the material stored inside the upper vertical module of the silo model, $W_{v1}$, and the area of the bin cross section, A. Because of the reduced dimensions of the silo model, it has been assumed the existence of a constant bulk density of the material [54] to determine the weight of the material existing at the hopper $W_h$ (Eq. 17), or a vertical section of a silo bin which is full of material ($g \cdot 0.5 \cdot V_v$).

$$p_{vt} = \frac{W_{vt} - W_h}{A} = \frac{\sum_{j=1}^{4} F_{Y3j} - \gamma \bullet V_h}{A} \quad (15)$$

$$p_{vv} = \frac{W_{v1}}{A} = \frac{W_{vt} - W_h - \gamma \bullet 0.5 \cdot V_v}{A} = \frac{\sum_{j=1}^{4} F_{Y3j} - \gamma \bullet (V_h + 0.5 \cdot V_v)}{A} \quad (16)$$

$$W_h = \gamma \bullet V_h \quad (17)$$

#### 2.2.5. Mass flow rate

Mass flow rate, Q, has been calculated (Eq. 18) by measuring the rate of change of the mass stored in the silo model for the time interval considered, $\Delta M_i$, with respect to that time interval, $\Delta t$.

$$Q = \frac{\Delta M_i}{\Delta t} \quad (18)$$

## 3. Results and discussion

### 3.1. Normal and tangential pressures on silo walls

Fig. 4 shows the evolution of the normal and tangential pressures recorded on the silo walls, in a representative replication of the assay for each hopper configuration analysed (0 %, 50 % and 100 % eccentricity). As indicated above, panels 1 and 3 are located on the walls farthest from the outlet orifice ($\theta = 180°$), while panels 2 and 4 are placed on the wall adjacent to the outlet ($\theta = 0°$). Panels 1 and 2 belong to the upper module of the silo and panels 3 and 4 to the lower module.

During the filling of the silo, in all the configurations analysed, a progressive increase in the pressures recorded in all the test panels was observed until a maximum value was reached at the end of the filling phase. Subsequently, during the 5-min resting phase, the normal and tangential pressure values remained relatively stable, which corroborates the findings reported in previous studies [1,38]. Once the resting period was completed, the silo was unloaded, registering a transient peak of the normal and tangential pressures at the beginning of emptying, in line with the observations of other authors [38,55–57], followed by a phase of greater variability in the measurements due to dynamic effects.

This trend only differs on the wall adjacent to the outlet orifice ($\theta = 0°$) in the lower module of the silo, where the opposite behaviour is observed, with an acute drop in pressures at the beginning of the discharge and a phase of subsequent fluctuations also attributable to the dynamic effects generated by the flow of material during the evacuation of the silo. Such behaviour pattern in the vicinity of the bin-hopper transition is consistent with previous observations made by other authors in funnel flow silos, where stress redistribution is strongly conditioned by the geometry of the hopper and the consolidation state of the bulk material [56 – 57].

As shown in Fig. 4, the values of the pressures recorded at the start of discharge in the upper module (sensors 1 and 2) are significantly higher than those recorded in the sensors of the lower module (3 and 4), regardless of the eccentricity of the hopper, which is in line with the results previously obtained by the authors in experimental tests carried out in the same silo prototype equipped with a flat bottom configuration [33]. It is worth pointing out that the pressures recorded in both panels located at the same height show some variability, even in the case of the centred hopper. These discrepancies may be associated with material movements and some eccentricity during filling and emptying, a phenomenon widely documented in granular materials, even under identical loading and unloading conditions [58].

Figs. 5 and 6 show respectively the evolution of the average normal and tangential pressures on the walls of the lower module of the silo (at a relative height of 0.17-H) during filling and emptying, obtained from the seven repetitions of the test carried out for each hopper eccentricity, where h/H is the relative height of pellets above the bin-hopper transition. The shaded areas show the standard deviation in each case.

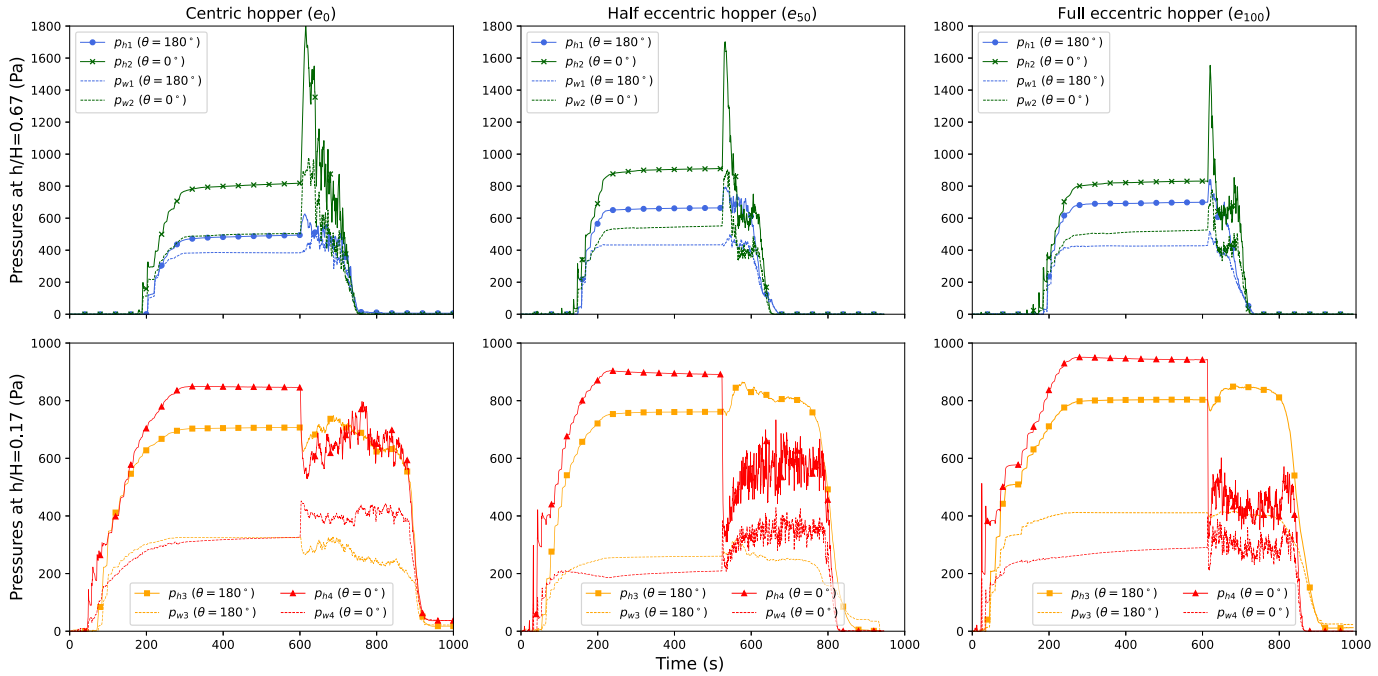


**Fig. 4.** Normal ($p_h$) and tangential pressures ($p_w$) on the silo walls measured in a representative test for each hopper configuration. From left to right: centred hopper ($e_0$), half-eccentric hopper ($e_{50}$) and full-eccentric hopper ($e_{100}$).

The readings show an appropriate repeatability of the tests, with coefficients of variation (CV) lower than 30 % for all the hopper configurations tested. The normal and tangential pressures existing on the two opposite walls of the silo during filling show certain differences, with the first offering slightly higher values on the wall adjacent to the outlet and slightly lower values for the second on the same wall ($\theta = 0º$). These asymmetries were also observed in the experimental tests carried out by Ramírez et al. [19] in hopper silos, although they were not observed in the experimental tests previously conducted by the authors with a flat bottom configuration [33].

Based on the above, it can be established that the presence of a hopper induces the occurrence of a transition zone in the material between different stress states, as well as the inclusion of a singularity in the wall geometry due to the change of inclination in its slope that would induce the occurrence of non-symmetrical pressure values even with the use of centred hoppers [59]. In addition, the inherent heterogeneity of granular materials and their properties may induce the occurrence of asymmetries in cases where they were not foreseeable [60 – 61].

During emptying, the eccentricity of the outlet orifice gives rise to significant differences in the pressures produced on the two opposite sides of the silo. The normal and tangential pressures tend to increase on the wall farthest from the outlet ($\theta = 180°$) as the eccentricity of the hopper increases, while a reduction in pressures is observed on the wall adjacent to the outlet ($\theta = 0°$). This trend agrees with experimental and numerical results obtained by other researchers [19,24,62]. Thus, the maximum normal pressure at the start of emptying (h/H = 1.0) goes from 614 Pa ($e_0$) to 750 Pa ($e_{100}$) for the wall farthest from the outlet ($\theta = 180°$), while at the opposite wall ($\theta = 0°$) it decreases from 574 Pa for the centred hopper ($e_0$) to 357 Pa for the full eccentric hopper ($e_{100}$).

### 3.2. Overpressures during emptying

Figs. 7 and 8 show the mean values of both normal and tangential pressures in the 4 test panels placed in the upper (h/H = 0.67) and lower (h/H = 0.17) module of the silo during filling ($p_{hf}$, $p_{wf}$) and discharge ($p_{hd}$, $p_{wd}$).

In the test panels located in the upper module of the silo (h/H = 0.67) the average normal and tangential pressures obtained during discharge exceed the pressures measured during filling for any of the relative pellet heights (h/H) considered. This consistent behaviour of the pressures in the upper part of the model silo is due to the existence in this zone of a mass flow, where the whole mass of the material is in motion [63 – 64].

However, the two measurement panels located in the lower module (h/H = 0.17) show a different behaviour depending on their location. The wall farthest from the outlet ($\theta = 180°$) exhibits a trend similar to that observed in the upper module, while the wall adjacent to the outlet ($\theta = 0°$) registered lower normal pressures during a part of the discharge than those obtained during filling for the same relative pellet height. This behaviour is consistent with previous work on eccentric hopper discharges where significant stress redistribution was identified, leading to a localised increase in pressures in certain structural regions [19].

The opening of outlet leads to the appearance of a free-falling column of the bulk material stored in the silo just above it. This causes a relaxation of the pressures applied over the silo wall, thus leading to a decrease of the wall normal pressures with respect to the existing ones at the rest state. This phenomenon increases as the outlet approaches to the silo wall (increased outlet eccentricity), as it can be observed in Fig. 7 at the wall adjacent to the outlet ($\theta = 0°$). At the same time, the movement of the pellets during the discharge increases the friction against the material that it is still trapped in the corrugations. This effect produces an increase in the internal friction between particles, thus leading to the increase of the wall frictional stresses during discharge (Fig. 8).

The hopper represents a geometric discontinuity that modifies the flow conditions, inducing the occurrence of transition zones in the stress state of the bulk material [65] and leading to the appearance of resting material zones whose amplitude varies depending on the inclination of the hopper [66]. The above results in higher fluctuations of pressure in the specific zone above and below the bin-hopper transition [30]. In addition, the eccentricity at the outlet induces even more significant changes in material flow, resulting in a major difficulty to predict pressure patterns.

Fig. 9 shows the values of the normal overpressure coefficients measured in the four instrumented panels. The results of the Tukey test showed the existence of statistically significant differences between the two walls, for both heights and in all hopper configurations ($p$-value $<0.002$ in all cases). Thus, the panels located in the upper module of the

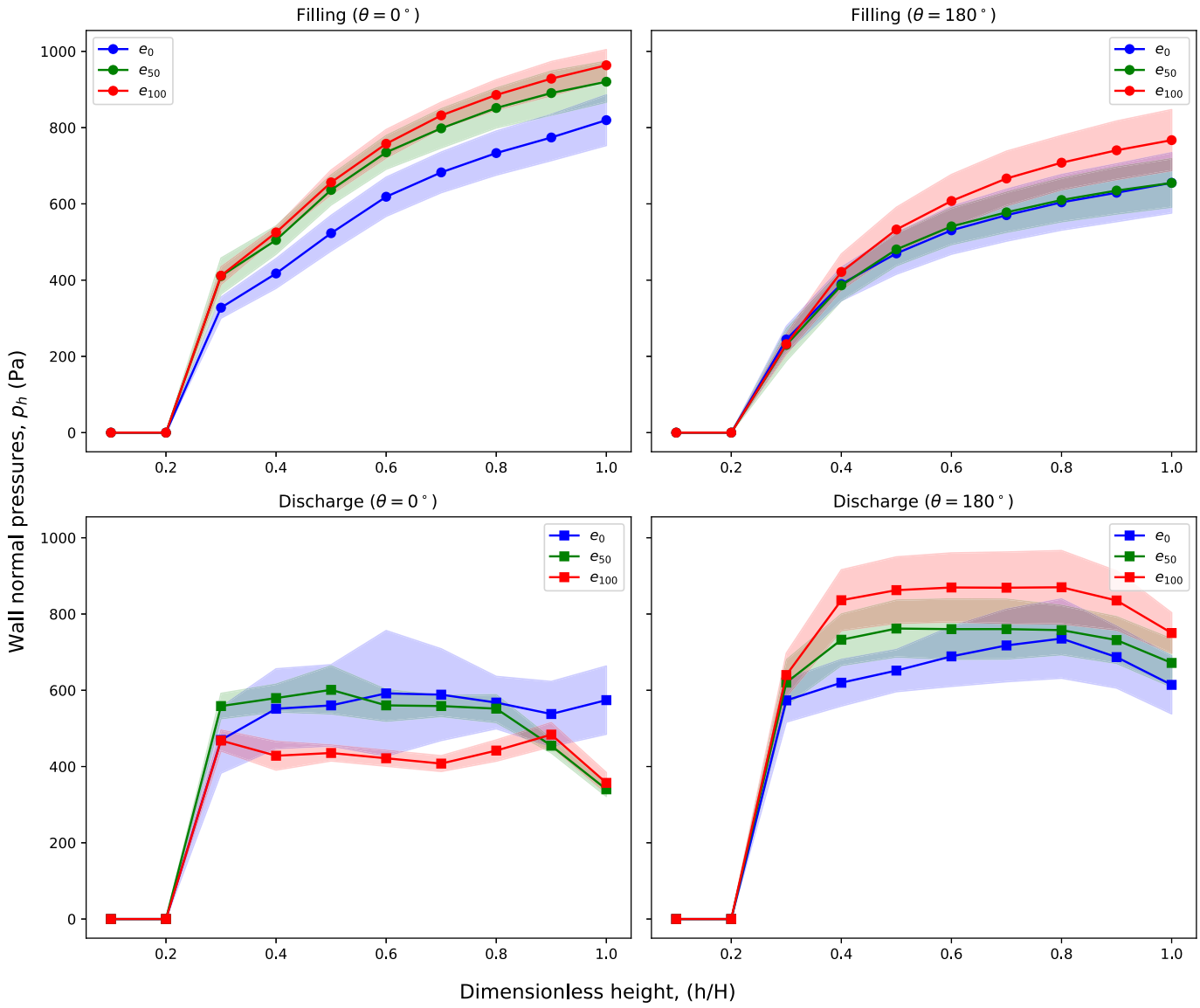


**Fig. 5.** Normal pressures ($p_h$) measured on the walls of the silo bottom module during filling (F) and discharge (D) versus the normalized height of stored material (h/H).

silo (h/H = 0.67) registered higher $C_{op,h}$ values on the wall adjacent to the outlet (θ = 0°) (mean values between 1.8 and 2.1) than those on the farthest wall (θ = 180°), where the mean measured value of $C_{op,h}$ ranged between 1.3 and 1.4. Higher values were obtained with the eccentric hoppers ($e_{50}$ and $e_{100}$) than in the centred hopper configuration ($e_0$). The overpressure coefficient obtained in the upper module (h/H = 0.67) for the half eccentric hopper ($e_{50}$) is significantly higher than the one corresponding to the full eccentric hopper. The existence of outlet eccentricity can lead to the appearance of non-symmetric flows of the bulk material during discharge, which can produce the appearance of unexpected effects. In any case, the asymmetry in the overpressures measured on both opposite walls may induce non-negligible bending moments structurally affecting the silo bin.

In contrast, the panels placed in the lower module of the silo (h/H = 0.17) showed a quite different behaviour, with higher overpressure coefficients on the most distant wall from the outlet (θ = 180°), with a $C_{op,h}$ value close to 1.2 for all the hopper configurations tested. On the other hand, in the wall adjacent to the outlet (θ =0°), the peak normal pressure during emptying was lower than the maximum value recorded during filling, thus obtaining overpressure coefficients inferior to 1 and progressively decreasing with increasing eccentricity, from 0.8 ($e_0$) to 0.5 ($e_{100}$). The results in the lower test panels are again influenced by the proximity to the bin-hopper transition, where the stress state of the material induces the appearance of asymmetries [30].

As the eccentricity of the hopper increases, during emptying the flowing granular material moves towards the wall adjacent to the outlet, so that in the case of the full eccentric hopper a column of pellets in full movement is placed above the outlet, meaning that the lateral pressure exerted on the wall adjacent to the outlet (θ = 0°) is significantly reduced. By contrast, the friction on that wall increases, as corroborated by Fig. 10, where the overpressure coefficients $C_{op,w}$ range between 1.2 and 1.6 on that wall (θ = 0°), being higher than the value recorded on the opposite wall (θ = 180°), ranging between 1 and 1.2.

In general, the tangential overpressure coefficients obtained (Fig. 10) are lower than the normal overpressure coefficients, except in the case described above. In the upper part of the silo (h/H = 0.67), again the wall near the outlet (θ = 0°) shows higher overpressure coefficients (mean values between 1.6 and 1.7) than those recorded on the opposite wall (mean values between 1.1 and 1.2). No significant differences due to hopper eccentricity are observed in the upper part of the silo.

The overpressure coefficients calculated according to EN 1991–4 depend on the eccentricity, both in the filling phase (considered centred

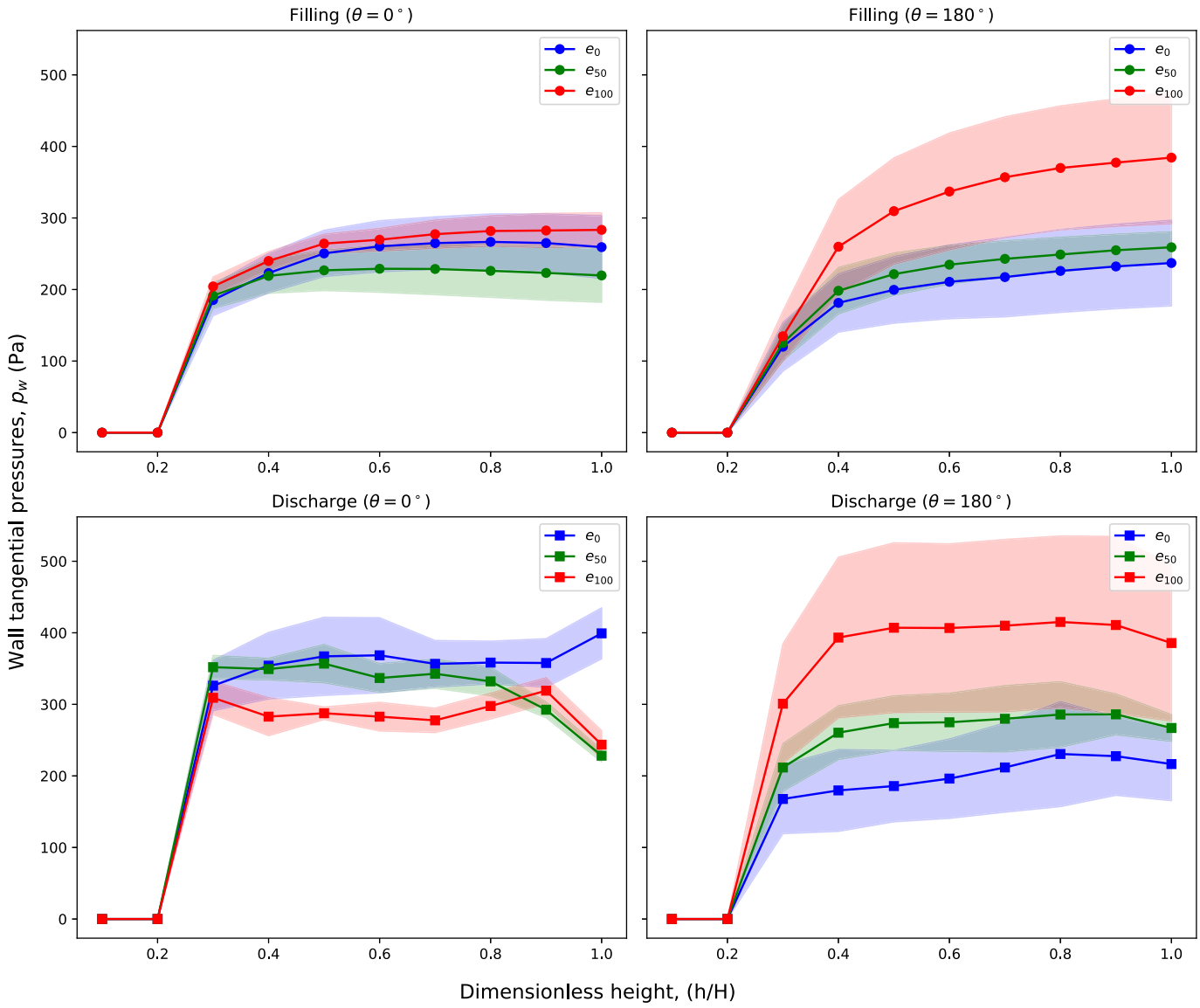


**Fig. 6.** Tangential pressures ($p_w$) measured on the walls of the silo bottom module during filling (F) and discharge (D) versus the normalized height of stored material (h/H).

in this analysis) and in the discharge, due to the hopper geometry. According to EN 1991–4, for a centred hopper slender silo ($e_0$) would be $C_w = 1.4$ for wall friction pressures and $C_h = 2.65$ for normal pressures, respectively increasing to $C_w = 1.52$ and $C_h = 2.78$ in a silo with 50 % eccentricity ($e_{50}$) and $C_w = 1.64$ and $C_h = 2.90$ in a full eccentric silo ($e_{100}$).

Fig. 11 compares the range of overpressure coefficients recorded in the experimental tests with those obtained according to EN 1991–4. The experimentally measured normal overpressure coefficients are lower than those calculated with Eurocode. However, in the case of tangential overpressure coefficients the experimentally obtained values (in the range 1.2–1.7) are similar and occasionally higher than those calculated with the Eurocode (in the range 1.4–1.6).

Table 2 shows a comparison of the overpressure coefficients obtained by the authors using the same model silo with a flat-bottom configuration and those recorded in this work with the hoppers indicated. In the upper section of the silo (Module 1), there are no significant differences in any case, with similar intervals for both overpressure coefficients. On the other hand, the differences are more appreciable in the lower test panel located on the wall adjacent to the outlet ($\theta = 0°$), where the effect of the bin-hopper transition is once again clear. Thus, in the case of the normal pressures, a coefficient $C_{op,h} = 1.1$ was obtained on both walls by using a flat bottom configuration, while coefficients below 1.0 were recorded in all configurations with hoppers. Similarly, in the case of the tangential pressures, the value obtained with the flat bottom silo was also $C_{op,w} = 1.1$, while using a hopper the registered value was in the range 1.2–1.6. In contrast, the differences were negligible on the opposite wall ($\theta = 180°$).

The observed differences in the values of the overpressure coefficients registered respectively at the top and bottom of the silo can be attributed to the propagation of rarefaction and compaction waves during the emptying stage, a phenomenon documented in other previous studies [67 – 68]. This phenomenon is also related to the well-known mixed flow, producing peak pressures at intermediate levels of the wall height [69 – 70]. Accordingly, at the beginning of the discharge, an overpressure is generated at the bottom of the silo, which propagates towards the top as a pressure wave, such that, in the upper module, the registered peak pressures can be comparable to the values measured at the base of the silo, and even, in some cases, higher. As the pressures exerted by the material in the upper region of the silo during the resting phase are considerably lower, significantly higher overpressure coefficients result in the upper module compared to the lower module.

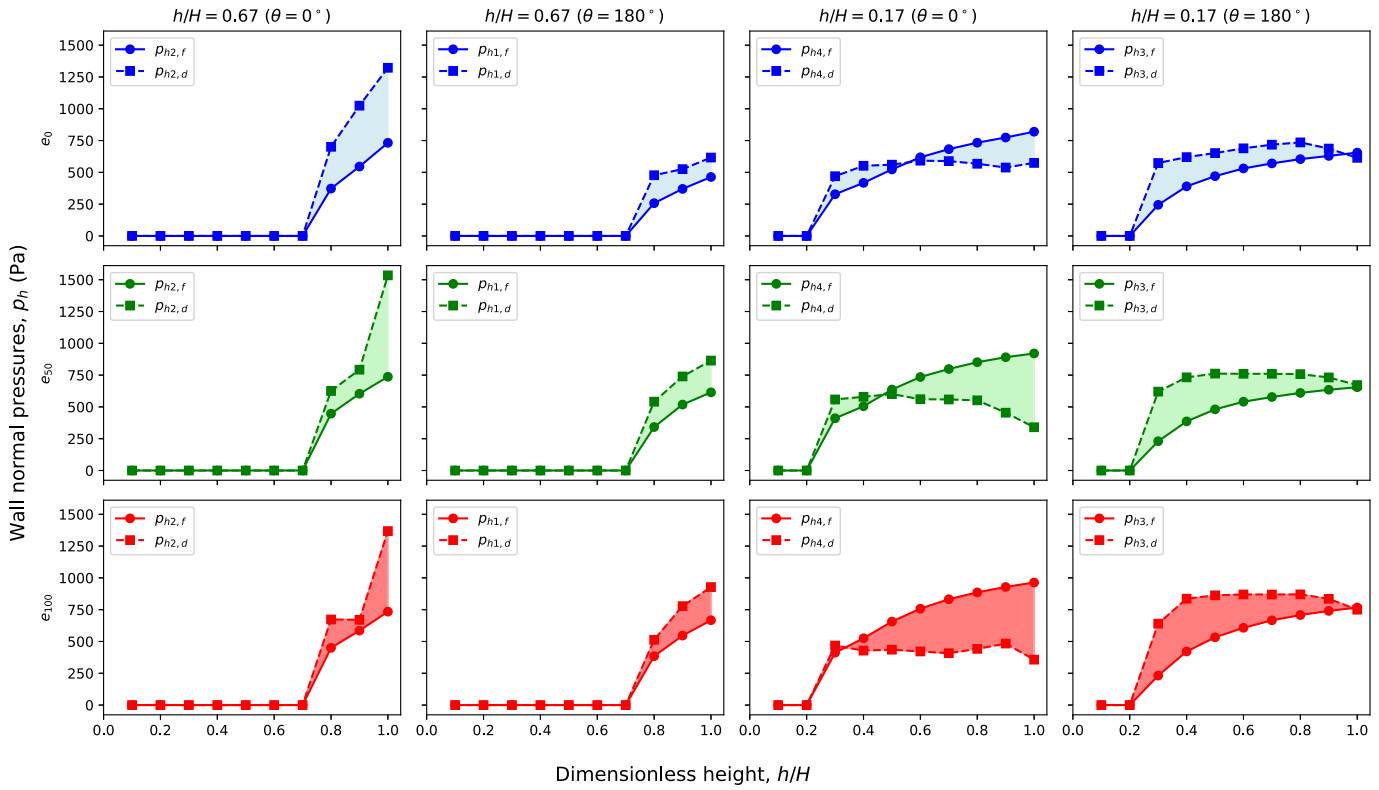


**Fig. 7.** Normal pressures ($p_h$) measured on both opposite walls of the silo ($\theta = 0°$ and $\theta = 180°$), versus the normalized height of stored material (h/H), at filling (F) and discharge (D). From top to bottom: centred hopper ($e_0$), semi-eccentric hopper ($e_{50}$) and full-eccentric hopper ($e_{100}$).

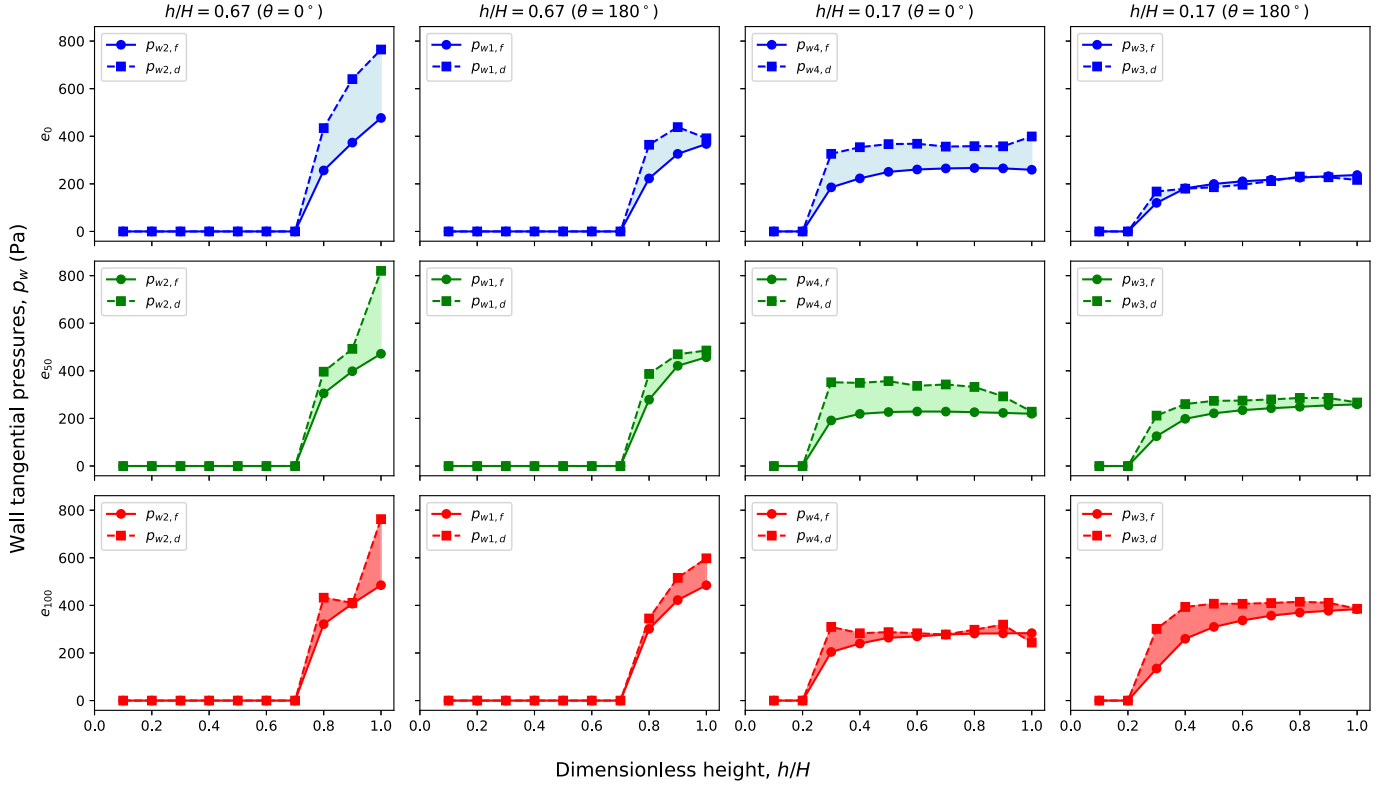


**Fig. 8.** Tangential pressures ($p_w$) measured on both opposite walls of the silo ($\theta = 0°$ and $\theta = 180°$), versus the normalized height of stored material (h/H), at filling (F) and discharge (D). From top to bottom: centred hopper ($e_0$), semi-eccentric hopper ($e_{50}$) and full-eccentric hopper ($e_{100}$).

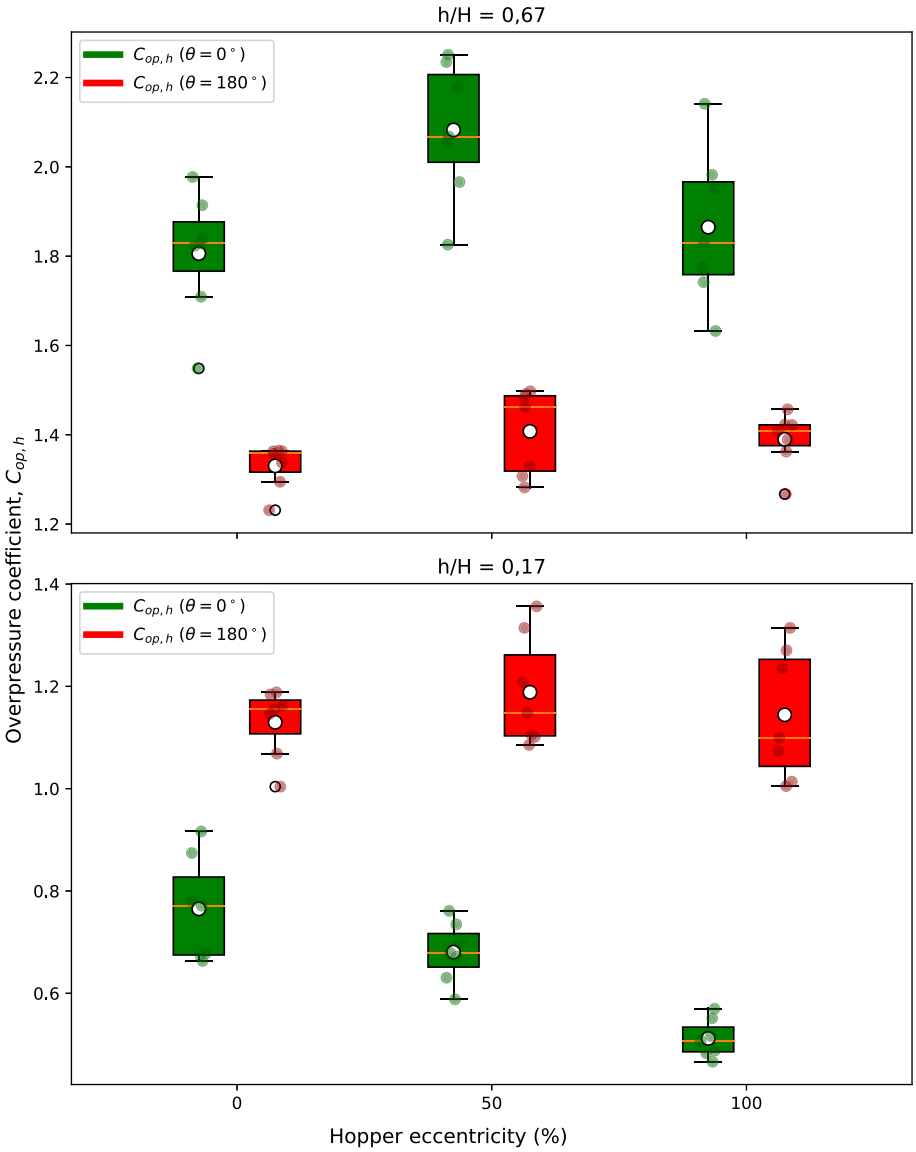


**Fig. 9.** Overpressure factors for normal pressures ($C_{op,h}$) for both opposite walls of the silo ($\theta = 0°$ and $\theta = 180°$).

### 3.3. *Effective wall friction coefficients*

Fig. 12 shows the evolution of the effective wall friction coefficient, experimentally obtained in a specific repetition of each test for the different hopper configurations analysed. The representativeness of this coefficient may not be appropriate during the initial stages of filling and the final moments of discharge because of the low pressures recorded and the variability in the measurements.

Fig. 13 shows the evolution of the effective coefficients of friction on the silo walls during filling and emptying for the three hopper configurations used in the experimental tests. On the other hand, the theoretical value according to EN 1991–4 (Eq. 12) that should be obtained with the tested material would be $\mu_{eff,EN} = 0.72$, considering the mechanical properties of the pinewood pellets tested ($a_w = 0.2$, $\phi_i = 39.5°$, $\mu_w = 0.30$).

The measured friction coefficients were higher in the upper vertical module (0.6–0.8) compared to the values recorded in the lower module (0.25–0.55) during the filling phase. The friction coefficients tend to be higher at the wall farthest from the outlet ($\theta = 180°$) compared to the closest wall ($\theta = 0°$) at both modules. On the other hand, the friction coefficient obtained in the lower module is significantly lower than the value predicted by the Eurocode or that obtained by the authors when using a flat bottom configuration [33], which again highlights the effect of the hopper on different parameters.

No significant differences were found during the discharge phase in those test panels located at h/H = 0.67, but there were differences in those test panels located close to the bin-hopper transition (at h/H = 0.17). It was observed an increase in the friction coefficient registered at the wall closest to the outlet ($\theta = 0°$) with respect to the resting phase, reaching values close to those registered in the upper test panels ($\mu_{eff}$ in the interval 0.6–0.8) but without any significant differences caused by the outlet eccentricity. These results agree with the findings reported in previous works, where a greater friction mobilization during the silo discharge was observed [1,31,71]. On the contrary, it was observed a decrease in the friction coefficient registered in the wall farthest from the outlet ($\theta = 180°$), with a slight increasing tendency with the increase in the outlet eccentricity ($\mu_{eff}$ between 0.25 and 0.4).

The total wall frictional forces measured in both vertical modules (Fig. 13) and the weight of the material resting on the silo bottom (Fig. 14) have been represented for a better understanding on the changes in the friction coefficient obtained. No significant differences were observed during filling, either between the two walls or due to the effect of the hopper eccentricity. Thus, the total wall frictional forces measured at any wall were approximately 210 N for the upper vertical

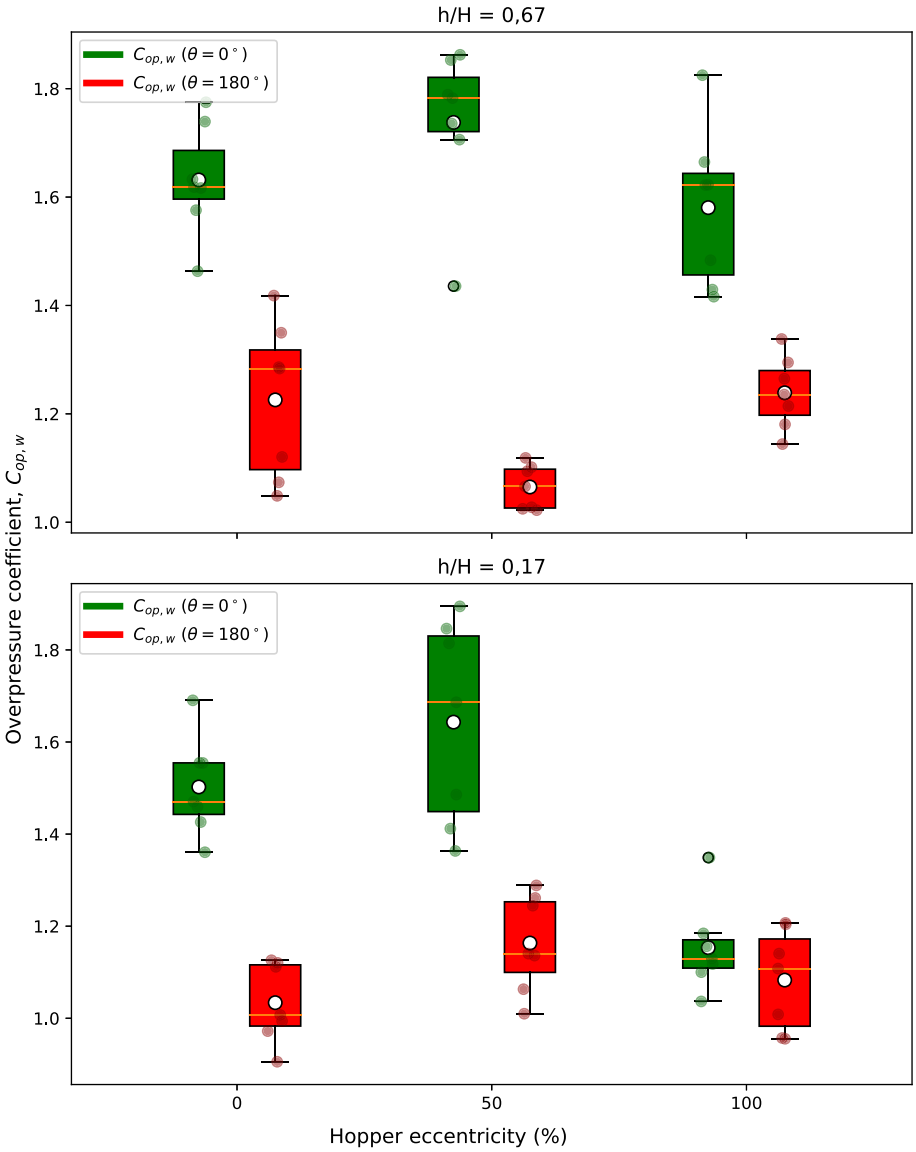


**Fig. 10.** Overpressure factors for tangential pressures ($C_{op,w}$) for both opposite walls of the silo ($\theta = 0°$ and $\theta = 180°$).

module ($F_{w1,f}$) and 330 N for the lowest vertical module ($F_{w2,f}$), while the material weight resting over the silo bottom was approximately 460 N ($F_{v,f}$).

A redistribution of forces is clearly observed during the silo discharge because a significant amount of the material weight is transferred to the walls. Therefore, a reduction in the weight resting over the silo bottom appears (Fig. 15), while an increase in the wall frictional forces is registered (Fig. 14), especially at the upper module. In addition, significant differences are observed during the emptying process in the upper module and the hopper.

A statistically significant influence of the outlet eccentricity was found at the upper module. The total frictional forces registered at both walls were 320 N at the beginning of discharge for the hopper $e_0$, while a difference of 40 N appeared between both walls (330 N at $\theta = 180°$ vs 290 N at $\theta = 0°$) for the hopper $e_{100}$. It can be observed that the difference in friction between both walls increases with the eccentricity of the hopper, with the friction being greater on the wall opposite to the outlet. On the other hand, it is interesting to note that in the lower module there are no significant differences in the friction between both walls, regardless of the eccentricity of the hopper.

The outlet induces a redistribution of the bulk mass stored in the silo, causing its centre of gravity to shift towards the opposite wall. In addition, the unloading process induces a change in the free surface of the material at the silo top, where the bulk solid stored descends more quickly on the wall near the outlet, which means a smaller amount of material is resting on the wall closest to the outlet. This phenomenon also explains why there is a very significant difference in the vertical component of the material weight resting over the silo bottom. The weight of the material is evenly distributed between both walls (345 N) at the silo bottom for the centric outlet ($e_0$), but the distribution is very uneven between both walls as the eccentricity of the hopper increases. For the case of the $e_{100}$ hopper, the wall farthest from the outlet ($\theta = 180°$) 390 N are supported, while only 310 N are supported in the wall closest to the outlet ($\theta = 0°$).

Fig. 16 shows the box-plot results of the effective wall friction coefficient obtained at the end of the resting phase and the beginning of discharge to analyse possible statistically significant differences between walls or silo locations. The outlet eccentricity has been found to have a positive significant influence on the friction coefficient only for the lower module (h/H = 0.17) and the wall opposite to the hopper outlet ($\theta = 180°$). In this case, increasing friction coefficients appear when increasing the outlet eccentricity. No significant differences between both walls appear at the upper module, with friction coefficients in the interval 0.55–0.8 for all hoppers tested. The values tend to be

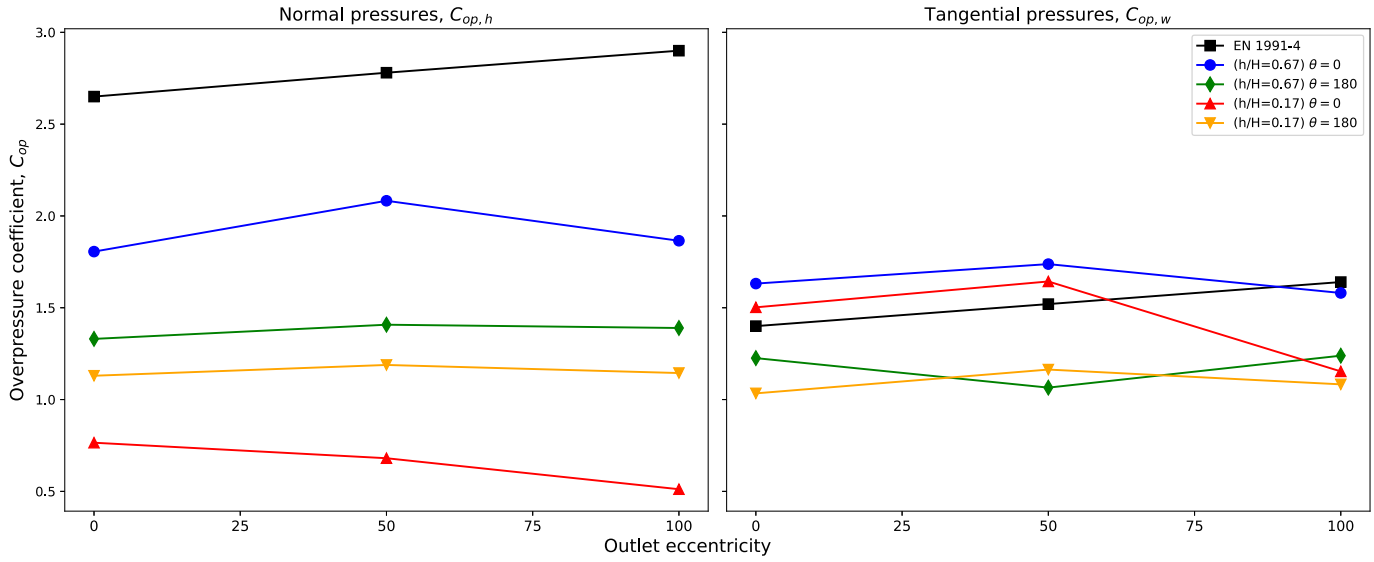


**Fig. 11.** Overpressure factors ($C_{op,h}$ and $C_{op,w}$) according to the relative height of stored material (h/H) and hopper eccentricity. Comparison with EN 1991–4.

**Table 2**
Comparison of mean value of overpressure coefficients ($C_{op,h}$ and $C_{op,w}$) in a flat-bottomed silo and in the different hopper configurations used in this work.

| Overpressure coefficient | Relative height (h/H) | Flat bottom Silo[a] | Hopper silo | |
|---|---|---|---|---|
| | | | Wall adjacent to the outlet (θ = 0°) | Wall farthest from the outlet (θ = 180°) |
| $C_{op,h}$ | 0.67 (Module 1) | 1.4–1.8 | 1.8–2.1 | 1.3–1.4 |
| | 0.17 (Module 2) | 1.1 | 0.5–0.8 | 1.2 |
| $C_{op,w}$ | 0.67 (Module 1) | 1.3–1.7 | 1.6–1.7 | 1.1–1.2 |
| | 0.17 (Module 2) | 1.1 | 1.2–1.6 | 1.1 |

[a] Taken from [33].

slightly greater in the wall located at (θ = 180°).

Significant differences have been found at the lower module (h/H = 0.17). The effective wall friction coefficients are in the range 0.3–0.5 during the filling phase in both walls, although with slightly higher values on the wall θ = 180°. At the beginning of the discharge phase, the value of the effective wall friction coefficient increases significantly in the panel closest to the outlet (θ = 0°), reaching a value of 0.7, while on the opposite wall the values are like those recorded at the end of filling. This significant increase in the friction coefficient does not occur because of the existence of a greater mobilization of friction in this module during unloading (see Figs. 7 and 12), but because of the decrease in the lateral pressures exerted by the bulk material on the wall (see Fig. 6), as a consequence of its proximity to the outlet.

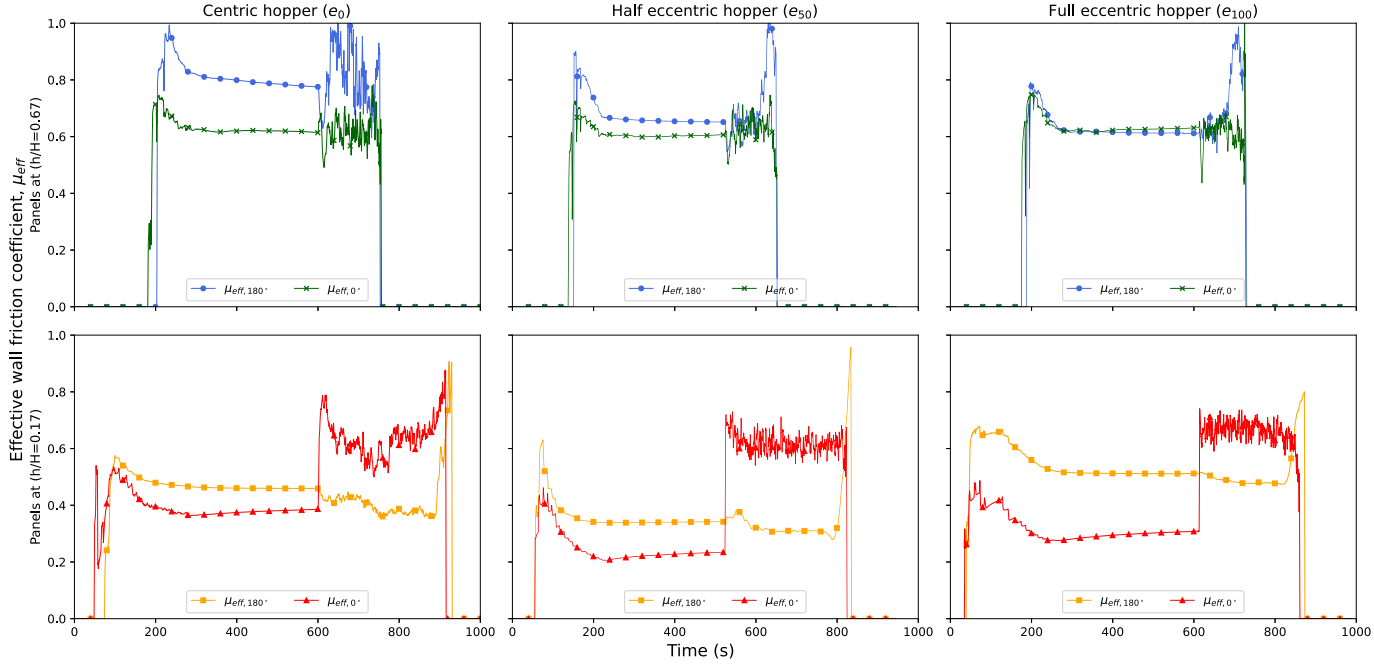


**Fig. 12.** Pellet-to-wall effective coefficient of friction ($\mu_{eff}$) obtained in a representative test for each hopper configuration.

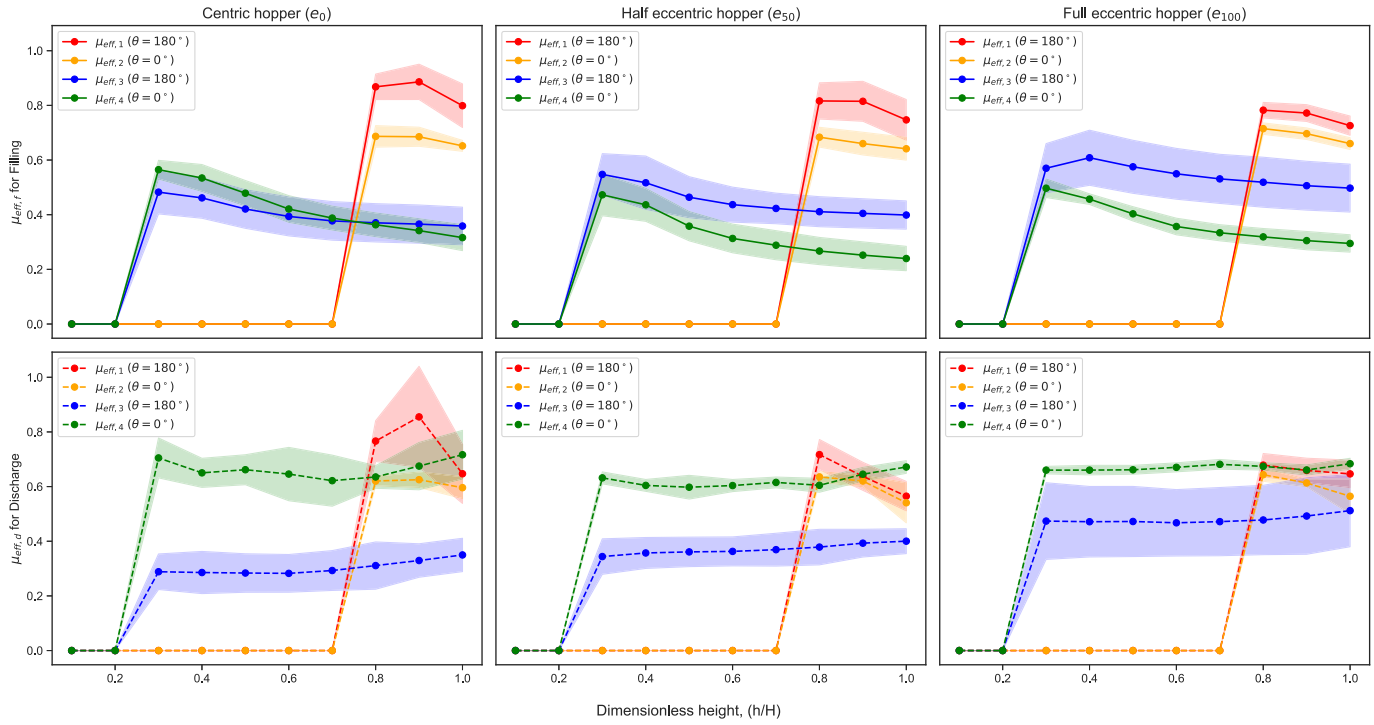


**Fig. 13.** Evolution of the effective wall friction coefficient ($\mu_{eff}$) versus the normalized height of stored material (h/H), at the top (panels 3 and 4) and bottom (panels 1 and 2) of the silo during filling (F) and discharge (D), for both opposite walls ($\theta = 0°$ and 180°). From left to right: centred hopper ($e_0$), semi-eccentric hopper ($e_{50}$) and full-eccentric hopper ($e_{100}$).

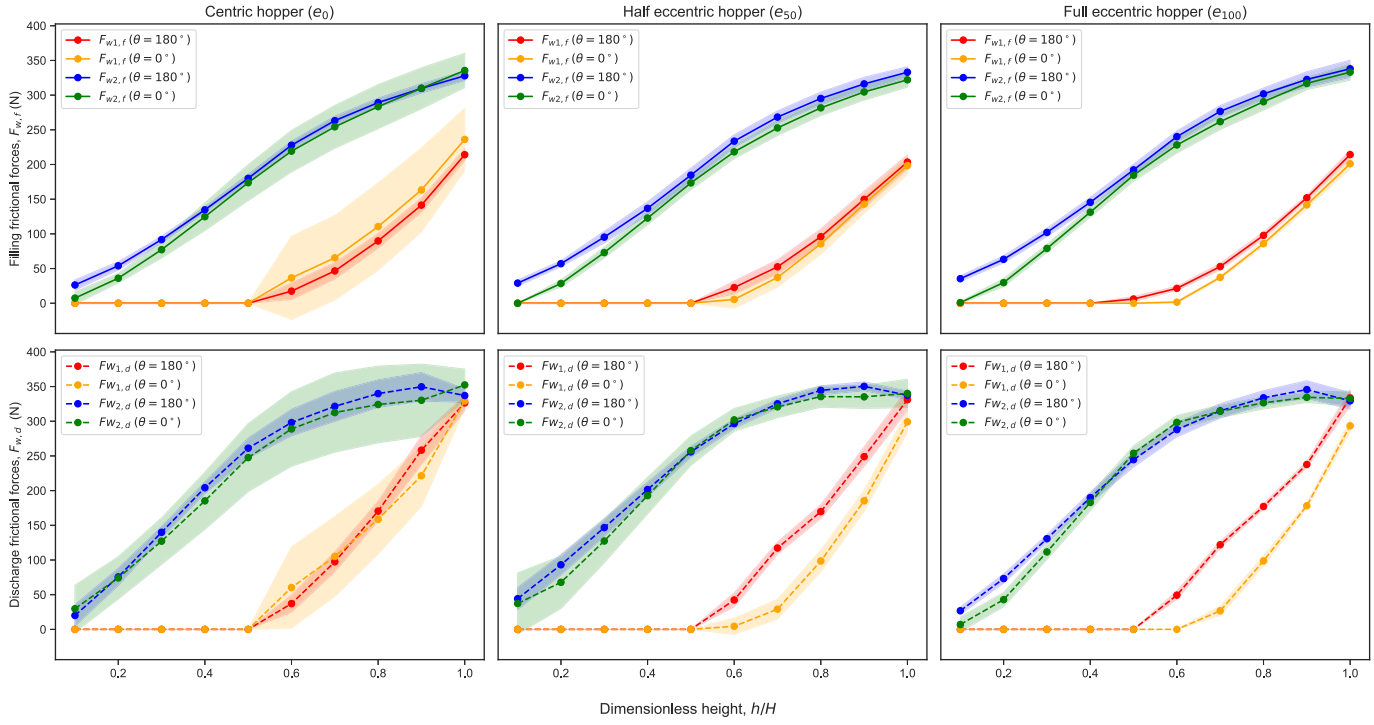


**Fig. 14.** Evolution of the wall frictional forces ($F_w$) versus the normalized height of stored material (h/H), at the upper (1) and lower (2) vertical modules of the silo during filling (F) and discharge (D), for both opposite walls ($\theta = 0°$ and 180°). From left to right: centred hopper ($e_0$), semi-eccentric hopper ($e_{50}$) and full-eccentric hopper ($e_{100}$).

### 3.4. *Lateral pressure ratio*

The values obtained for the lateral pressure ratio, K, at the location of the test panels for all hoppers considered are shown in Fig. 17, where $K_3$ and $K_4$ refer to test panels placed in the lowest module (h/H = 0.17), while $K_1$ and $K_2$ correspond to test panels placed in the uppermost module (h/H = 0.67). K values remain quite stable during the filling and resting phase for all locations and hopper configurations, with values

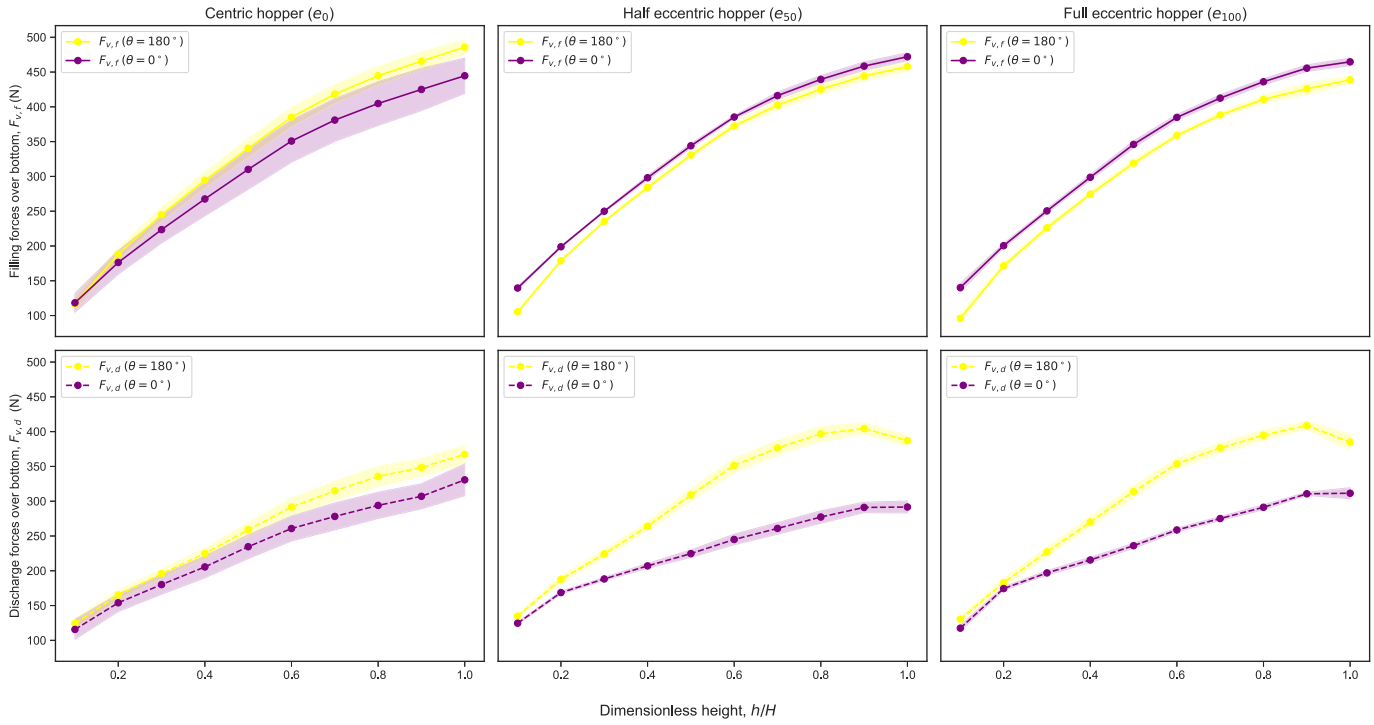


**Fig. 15.** Evolution of the forces over silo bottom ($F_v$), versus the normalized height of stored material (h/H) during filling (F) and discharge (D). From left to right: centred hopper ($e_0$), semi-eccentric hopper ($e_{50}$) and full-eccentric hopper ($e_{100}$).

ranging in the interval 0.15–0.23. This value is significantly lower than the one obtained according to EN 1991–4 ($K_{EN} = 0.38$) or the coefficient of pressure at rest ($K = 0.35$), which are estimated from the angle of internal friction of the material ($\phi_i = 39.5°$). An active stress state exists in the bulk material during the resting phase [59]. So, the value obtained from the Rankine coefficient for active pressure ($K = 0.21$) agrees well with the ones experimentally obtained.

The lateral pressure ratio proposed by Drescher [59] for bins by assuming the existence of material yielding at the wall and an active stress state ($K = 0.20$) is also consistent with the experimental values obtained. The assumption of material yielded in the region close to the corrugated wall is based on the findings of the previous numerical works developed by the authors [43].

The values calculated for K during silo emptying show significant differences. On the one hand, the values obtained for discharge are significantly greater than those existing for filling, which is a finding previously observed by other authors [7,56,65]. On the other hand, significantly larger values (K peak value of 0.93) are reported for test panels located at h/H = 0.67 in comparison with those obtained at h/H = 0.17 (peak value close to K = 0.4). This can be explained because of the relative increase of the lateral pressure is greater for upper test panels than for lower test panels (greater overpressure coefficients, as shown in section 3.2), and the weight of the material over this location is significantly lower than the existing at bin–hopper transition. This finding was also reported by Gandia et al. [56], who found increasing values for K when decreasing the silo slenderness (H/D, where H is the material height and D is the silo diameter) of bin-hopper silos filled with maize kernels. In addition, the peak K value reported for discharge is close to the value (K = 0.8) proposed by Drescher [59] when considering a passive stress state (the one existing in the bulk material during silo emptying) and a material yielding close to the silo wall.

Finally, the Tukey tests conducted have found a statistically significant influence of hopper eccentricity on the K values for both walls obtained at h/H = 0.17. Thus, if a centric outlet ($e_0$) is considered, no differences between both walls are reported, and the K value slightly vary from 0.22 (at the start of discharge) up to a peak value of 0.38 during discharge. A similar trend and K values are observed for the eccentric hoppers ($e_{50}$, $e_{100}$) only for the wall opposite to the outlet ($\theta = 180°$). The K values obtained at test panel located at the wall closest to the outlet ($\theta = 0°$) are lower, and the difference between both walls increases when increasing the outlet eccentricity. Thus, a peak value of $K = 0.25$ is found for $e_{100}$ and $\theta = 0°$, which is significantly lower than the one obtained at $\theta = 180°$ ($K = 0.4$).

The slight increase of K during the emptying phase can be attributed to the fact that the relaxation of lateral pressures is slower than the decrease in the vertical pressure. On the other hand, the asymmetry in the K values between both walls for eccentric hoppers is explained because of the previously described asymmetric patterns of pressures reported, as a consequence of the changes in the flow regime caused by the outlet eccentricity.

### 3.5. *Mass flow rate*

Fig. 18 shows the evolution of the mean and standard deviation (shadowed area) mass flow rate during discharge for all the hoppers analysed. The values corresponding to the start and end of the discharge process were not considered in calculations to avoid the appearance of disturbances in the parameter. Thus, results are obtained for the 90 % of the discharge process. The results obtained in all tests are very consistent and low standard deviations exist for all hoppers. A decrease of mass flow rate at the end of discharge could be observed, confirming previous findings by [1,33].

The Tukey test conducted did not show the existence of significant differences between the centric ($e_0$) and half eccentric ($e_{50}$) hoppers, with mean mass flow rates of 0.482 and 0.478 kg/s during the discharge phase, respectively. However, significant differences were reported between the full eccentric hopper ($e_{100}$) and the other ones. In this case, the mean mass flow rate measured during discharge was 0.53 kg/s. It is well known that mass flow rate is basically governed by the particle size, the outlet width or the silo dimensions [72], but the angle of inclination in bevelled silo outlet [73] or even the wall friction coefficient [74] can also affect the mass flow rate.

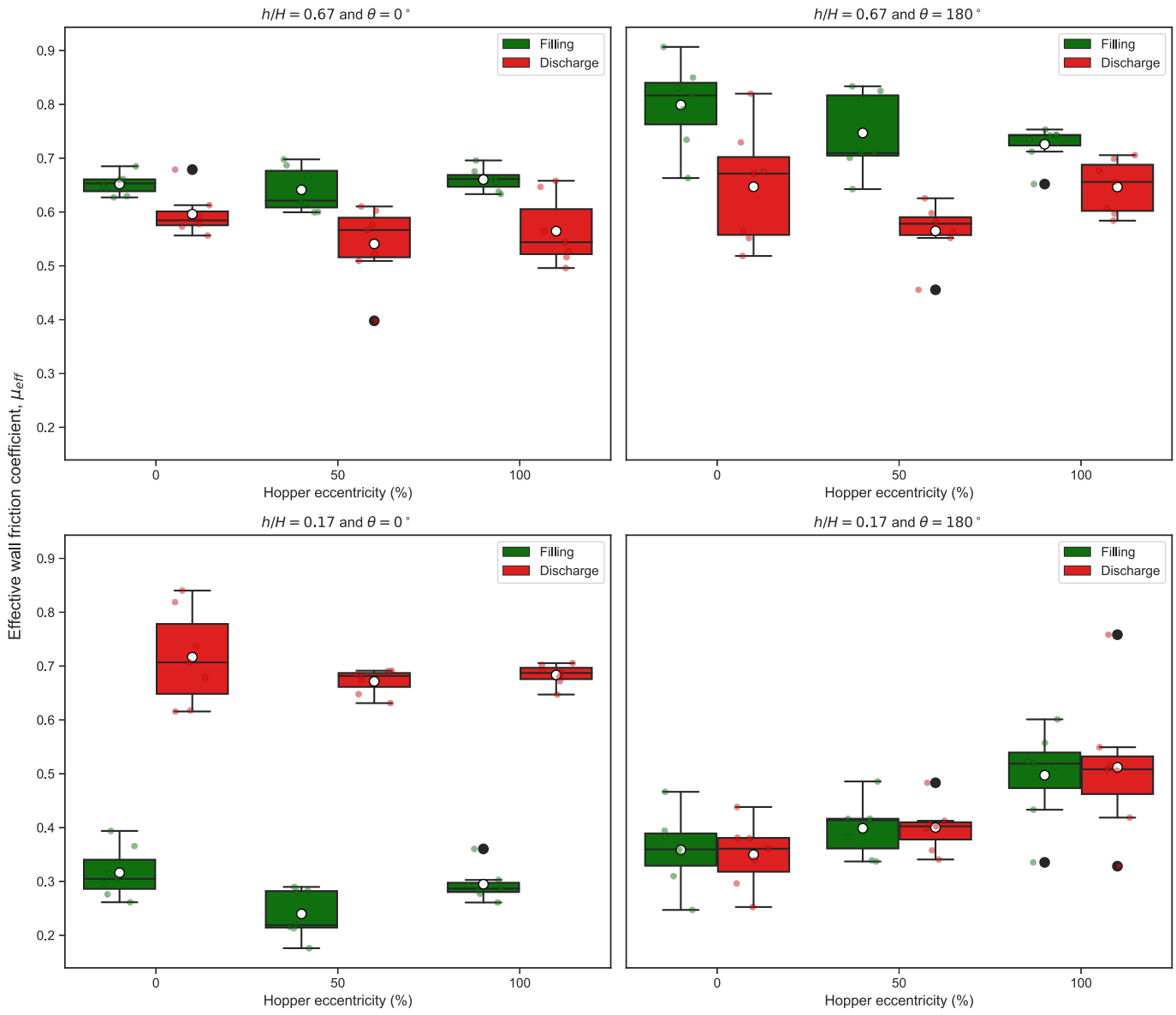


**Fig. 16.** Box plot showing the effective wall friction coefficient ($\mu_{eff}$) versus hopper eccentricity ($e_0$, $e_{50}$, $e_{100}$) at the end of filling/beginning of discharge, for both opposite walls ($\theta = 0°$ and 180°), at the upper (h/H = 0.67) and lower (h/H = 0.17) vertical modules of the silo.

The findings obtained in the experimental tests matches the observations of Wang et al. [75], who also observed a positive effect of outlet eccentricity in the mass flow rate when a critical eccentricity of 80 % was exceeded. Below the threshold value of the critical eccentricity, no significant changes in the flow of particles appear, thus leading to negligible changes in the mass flow rate. Thus, this explains why no significant differences have been found between hoppers with 0 % ($e_0$) and 50 % ($e_{50}$) outlet eccentricities, while significant changes were found for the full eccentric hopper ($e_{100}$).

## 4. Conclusions

The results obtained in this study show the significant effects that hopper eccentricity produces in the redistribution of forces over the silo walls and bottom, which can be of importance for a proper design of these structures. The main findings of this work are as follows:

- Increasing outlet eccentricity leads to a 33 % decrease in the mean values of wall normal pressures obtained in the test repetitions conducted (from 600 Pa to 400 Pa) at the wall closest to the outlet ($\theta = 0°$) during discharge, while a significant 33 % increase in normal pressures (from 600 Pa to 800 Pa) appears at the opposite wall ($\theta = 180°$). This effect was also observed for the wall tangential pressures, thus leading in both cases to an asymmetric distribution of wall pressures.
- The overpressure coefficients obtained for the wall normal pressures are significantly lower (below 2.1) than those predicted by EN 1991–4 (2.65–2.9 interval), while similar values were obtained for wall tangential pressures (close to 1.5). Additionally, the higher the outlet eccentricity, the lower the overpressure coefficient is reported at the wall closest to the outlet and in the lower vertical module (h/H = 0.17).
- The friction coefficients measured were higher in the upper part of the silo (from 0.6 to 0.8) compared to the values recorded in the lower module (from 0.25 to 0.55) during the filling phase. The friction coefficients tended to be higher at the wall farthest from the outlet ($\theta = 180°$) compared to those registered at the closest wall ($\theta = 0°$) for both modules. No significant differences were found during the discharge in the test panels located in the upper module, but an increase in the friction coefficient appeared in those located near the

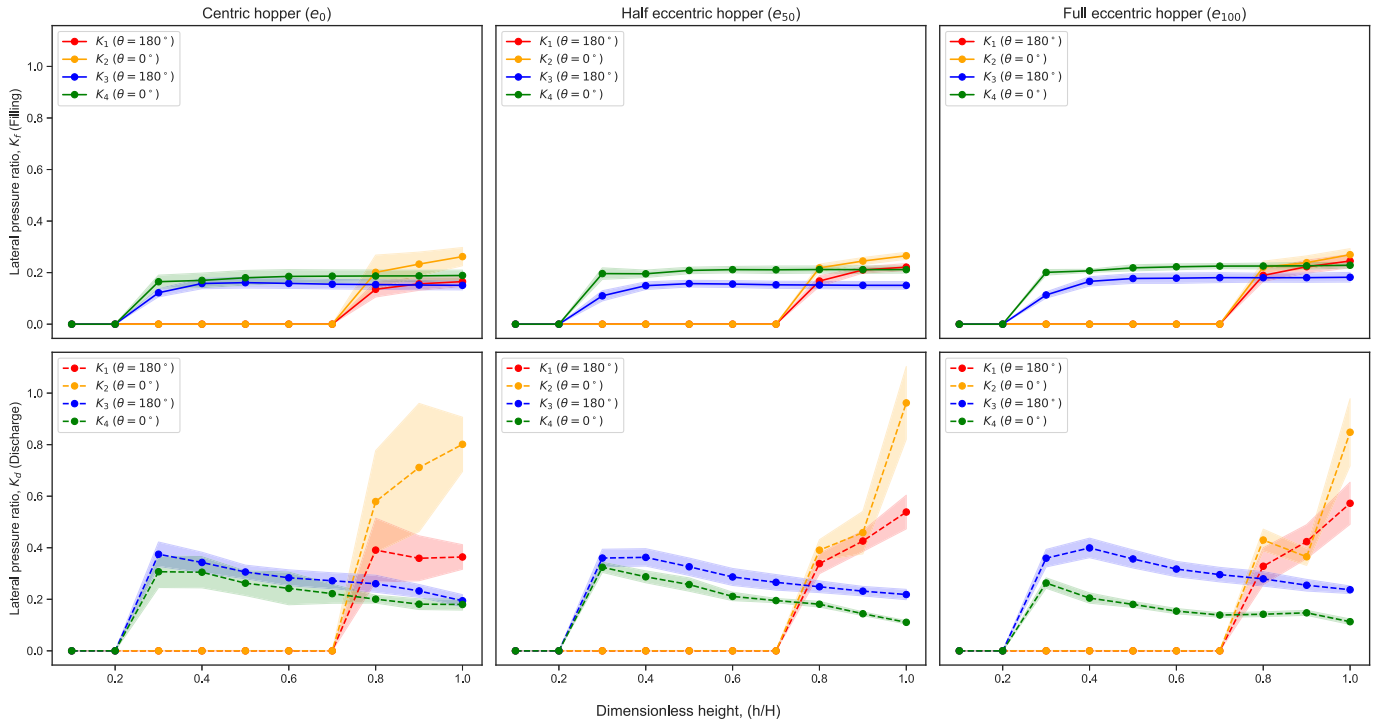


**Fig. 17.** Evolution of the lateral pressure ratio (K) versus the normalized height of stored material (h/H), at the top (panels 3 and 4) and bottom (panels 1 and 2) of the silo during filling (F) and discharge (D), for both opposite walls (θ = 0° and 180°). From left to right: centred hopper ($e_0$), semi-eccentric hopper ($e_{50}$) and full-eccentric hopper ($e_{100}$).

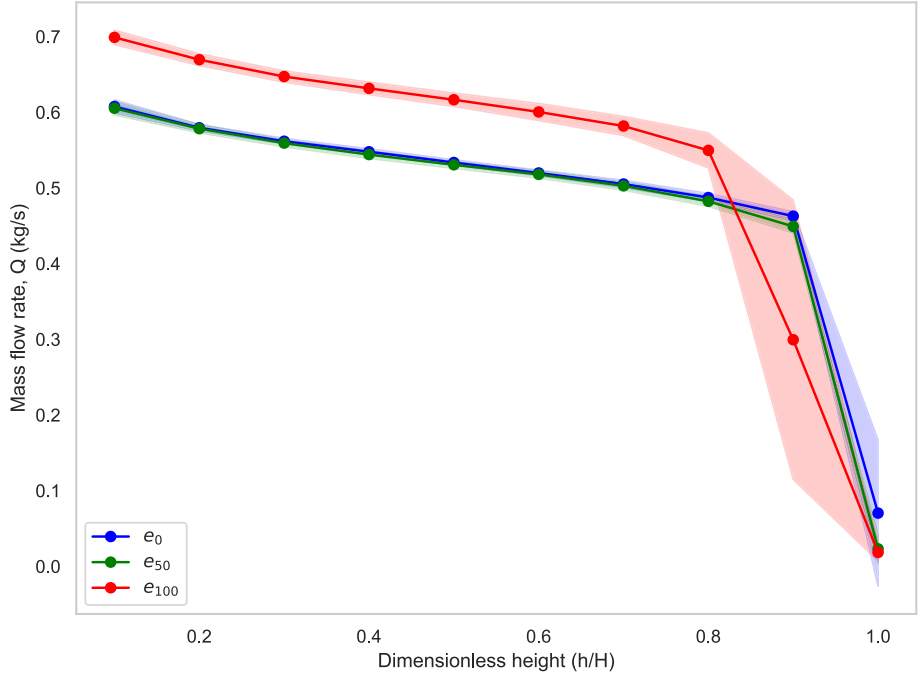


**Fig. 18.** Mass flow rate during discharge (Q) versus normalized height of stored material (h/H), for the three different hopper configurations tested ($e_0$, $e_{50}$ and $e_{100}$).

bin-hopper transition, the effect being more pronounced in the wall closest to the outlet (θ = 0°).

- The outlet eccentricity induces a redistribution of the bulk mass stored in the silo during the discharge process, then inducing an increase in the frictional forces at the wall farthest from the outlet in the vertical upper module. In addition, the increase in outlet eccentricity also increases the fraction of the material weight resting over the silo bottom at the location farthest from the outlet. For example, the weight resting over the silo bottom at θ = 180° increases from 345 N for the centred hopper up to 390 N for the full-eccentric hopper.
- Outlet eccentricity also produces statistically significant differences at h/H = 0.17 between the lateral pressure ratios (K) measured for

both walls. This difference can be basically attributed to the increase of K at wall θ = 180° with increasing outlet eccentricities.

- The mean mass flow rate obtained for the full-eccentric hopper (0.53 kg/s) is significantly higher than the one reported for the other hoppers (0.48 kg/s). This finding corroborates previous results of Wang et al. [75] with regards to the existence of a critical eccentricity affecting the flow conditions existing within the silo.

The reduced dimensions of the silo model employed might produce scale effects that should be considered. Therefore, experimental tests in full scale silos would be recommended to generalize the conclusions obtained in this work. At the same time, additional tests would be required to generalize the findings of the paper by testing different materials, particle shapes or silo wall characteristics (the corrugation wavelength and depth).

## List of Symbols

| | |
|---|---|
| $F_{Xi}$ | Lateral force, measured in N, recorded at panel position i (i = panels 1 to 4 in the present model) at time t |
| $F_{Yi}$ | Vertical force, measured in N, recorded at panel position i (i = panels 1 to 4 in the present model) at time t |
| $F_{Yij}$ | Vertical force, measured in N, recorded by sensors at level i (i = sensors 1 to 3), and position j (j = panels 1 to 4 in the present work) at time t |
| $M_t$ | mass of the stored material at time t (kg) |
| $W_t$ | weight of the stored material at time t (N) |
| $W_{vv}$ | weight of the stored material in the vertical body at time t (N) |
| $W_{v1}$ | weight of the material stored in the upper vertical module of the silo model |
| $W_{vt}$ | weight of the stored material at the silo bottom (or the transition with the hopper should there be one) at time t (N) |
| $W_h$ | weight of the material in the hopper at time t (N) |
| V | total volume of the silo model ($m^3$) ($V = 0.3066\ m^3$) |
| $h_i$ | height of the stored material at the silo bottom (or the transition with the hopper should there be one) at time t (m) |
| $V_v$ | interior volume of the vertical body of the model silo ($m^3$) ($V_v = 0.2954\ m^3$) |
| $V_h$ | interior volume of the hopper when using a hopper configuration ($m^3$) ($V_h = 0.0112\ m^3$) |
| $M_h$ | mass of the material stored inside the hopper (kg) |
| $\gamma$ | bulk specific weight of the stored material ($kN/m^3$) |
| $\mu_{effi}$ | effective friction coefficient at the corrugated steel wall measured at panel position i at time t |
| $p_{hi}$ | normal pressure caused by the stored material at panel position i (i = panels 1 to 4 in the present work) at time t (Pa) |
| $p_{wi}$ | tangential pressure caused by the stored material at panel position i (i = panels 1 to 4 in the present work) at time t (Pa) |
| $p_{vt}$ | vertical pressure existing at bin-hopper transition at time t (Pa) |
| $p_{vv}$ | vertical pressure at the transition between the vertical body modules at time t (Pa) |
| $A_p$ | effective surface area of the test panel ($A_p = 0.0222\ m^2$) |
| A | interior area of the cross section of the vertical body of the model silo ($A = 0.197\ m^2$) |
| H | total height of vertical silo modules (H = 1,5 m). |
| L | width and length of the square cross section of the silo model (L = 0,45 m). |
| U | perimeter of the cross section of the model silo (U = 1.776 m) |
| $K_i$ | lateral-to-vertical pressure ratio |
| $F_{w1}$ | total frictional force recorded in the upper vertical body module at time t (N) |
| $F_{w1R}$ | total frictional force recorded in the upper vertical body module, on the right side of the silo (θ = 180°), at time t (N) |
| $F_{w1L}$ | total frictional force recorded in the upper vertical body module, on the left side of the silo (θ = 0°), at time t (N) |
| $F_{w2}$ | total frictional force recorded in the lower vertical body module at time t (N) |
| $F_{w2R}$ | total frictional force recorded in the lower vertical body module, on the right side of the silo (θ = 180°), at time t (N) |
| $F_{w2L}$ | total frictional force recorded in the lower vertical body module, on the left side of the silo (θ = 0°), at time t (N) |
| Q | mass flow rate (kg/s) |
| $C_{op,h}$ | Overpressure coefficient of normal pressures measured in the beginning of discharge |
| $C_{op,w}$ | Overpressure coefficient of wall tangential pressures measured in the beginning of discharge |

## CRediT authorship contribution statement

**Adriano Pinilla:** Writing – original draft, Investigation, Data curation. **José María Fuentes:** Writing – review & editing, Methodology, Formal analysis. **Francisco Ayuga:** Project administration, Funding acquisition. **Eutiquio Gallego:** Writing – review & editing, Supervision, Funding acquisition, Conceptualization.

## Declaration of competing interest

The authors declare the following financial interests/personal relationships which may be considered as potential competing interests:

Eutiquio Gallego Vazquez reports financial support was provided by the Spanish Agencia Estatal de Investigación. If there are other authors, they declare that they have no known competing financial interests or personal relationships that could have appeared to influence the work reported in this paper.

## Data availability

All data used during this study are available at the repository included in e-cienciaDatosfrom Consorcio Madroño (https://doi.org/10.21950/TC0EB4).

## Acknowledgements

This research was funded by the Spanish Agencia Estatal de Investigación via the research project “Study of the structural behaviour of corrugated wall silos using Discrete Element Models (SILODEM)” (grant number PID2019-107051 GBI00/AEI/10.13039/501100011033). The authors also thank the SYMAGA S.A. company for providing the corrugated steel sheets employed in the silo model.

## References

[1] J. Wiącek, E. Gallego, P. Parafiniuk, R. Kobyłka, M. Bańda, J. Horabik, M. Molenda, Experimental analysis of wheat-wall friction and grain flow in a steel silo with corrugated walls, Biosyst. Eng. 209 (2021) 216–231, https://doi.org/10.1016/j.biosystemseng.2021.07.003.

[2] CEN (Ed.), EN 1991–4. Eurocode 1 - Actions on Structures - Part 4: Silos and Tanks, 1st ed., CEN, Brussels, 2006.

[3] D.M. Walker, An approximate theory for pressures and arching in hoppers, Chem. Eng. Sci. 21 (1966) 975–997, https://doi.org/10.1016/0009-2509(66)85095-9.

[4] A. Dąbrowski, Pressures in bulk solids in hoppers (in polish), Arch. Inżynierii Lądowej 3 (1957) 325–334.

[5] V. Askegaard, J. Munch-Andersen, Results from tests with normal and shear stress cells in a medium-scale model silo, Powder Technol. 44 (1985) 151–157, https://doi.org/10.1016/0032-5910(85)87022-4.

[6] C.J. Brown, E.H. Lahlouh, J.M. Rotter, Experiments on a square planform Silo, Chem. Eng. Sci. 55 (2000) 4399–4413, https://doi.org/10.1016/S0009-2509(99)00574-6.

[7] A. Couto, A. Ruiz, P.J. Aguado, Experimental study of the pressures exerted by wheat stored in slender cylindrical silos, varying the flow rate of material during discharge. Comparison with Eurocode 1 part 4, Powder Technol. 237 (2013) 450–467, https://doi.org/10.1016/j.powtec.2012.12.030.

[8] K.C. Dornelas, H.C. Soares Rodrigues, A.B. Cheung, C.C. Junior, J.W. Barbosa do Nascimento, Pressures in squat steel silo with flat bottom storing maize grain,

J. Stored Prod. Res. 109 (2024) 102424, https://doi.org/10.1016/j.jspr.2024.102424.
[9] R.M. Gandia, F.C. Gomes, W.C. de Paula, P.J.A. Rodriguez, The influence of flow pattern and hopper angle on static and dynamic pressures in slender silos, Powder Technol. 427 (2023) 118756, https://doi.org/10.1016/j.powtec.2023.118756.
[10] M. Molenda, M.D. Montross, S.A. Thompson, J. Horabik, Asymmetry of model bin wall loads and lateral pressure induced from two- and three-dimensional obstructions attached to the wall, Trans. ASABE 52 (2009) 225–233, https://doi.org/10.13031/2013.19908.
[11] J.W.B. Nascimento, J.P. Lopes Neto, M.D. Montross, Horizontal pressures in cylindrical metal silos and comparison with different international standards, Engenharia Agrícola 33 (2013) 601–611, https://doi.org/10.1590/S0100-69162013000400002.
[12] B.A. Petrov, Experimental determination of central pressure of reinforced concrete silo walls (experimental noe Opredelenie davlenia Cementa na StenkiZhelezobetonnich Silosov), Cement 2 (1958) 21–25.
[13] M.L. Reimbert, A.M. Reimbert, Silos: Theory and Practice, Trans Tech Publications, 1976.
[14] M. Sugita, Flow and pressures of noncohesive granular materials in funnel-flow bins, in: Presented at the Mechanical Engineering, ASME-AMER SOC MECHANICAL ENG 345 E 47TH ST vol. 10017, 1972, p. 60. NEW YORK, NY.
[15] R. Aoki, H. Tsunakawa, The pressure in a granular material at the wall of bins and hoppers, J. Chem. Eng. Jpn 2 (1969) 126–129, https://doi.org/10.1252/jcej.2.126.
[16] S. Ding, Y. Ji, S. Ye, J.M. Rotter, Q. Li, Measurements of pressure and frictional tractions along walls of a large-scale conical shallow hopper and comparison with Eurocode 1991-4:2006, Thin-Walled Struct. 80 (2014) 231–238, https://doi.org/10.1016/j.tws.2014.03.008.
[17] J. Munch-Andersen, Silo model tests with sand, SBI-meddelelse no. 91, SBI forlag, 1992.
[18] A. Ramírez, J. Nielsen, F. Ayuga, On the use of plate-type normal pressure cells in silos. Part 1: calibration and evaluation, Comput. Electron. Agric. 71 (1) (2010) 71–76, https://doi.org/10.1016/j.compag.2009.12.004.
[19] A. Ramírez, J. Nielsen, F. Ayuga, Pressure measurements in steel silos with eccentric hoppers, Powder Technol. 201 (1) (2010) 7–20, https://doi.org/10.1016/j.powtec.2010.02.027.
[20] J.M. Rotter, Guide for the Economic Design of Circular Metal Silos, CRC Press, 2001.
[21] A.J. Matchett, J. O'Neill, A.P. Shaw, Stresses in bulk solids in wedge hoppers: A flexible formulation of the co-ordinate specific, Lame–Maxwell equations for circular arc, principal stress systems, Powder Technol. 194 (2009) 166–180, https://doi.org/10.1016/j.powtec.2009.04.002.
[22] R.L. Michalowski, Approximate theory of loads in plane asymmetrical converging hoppers, Powder Technol. 36 (1983) 5–11, https://doi.org/10.1016/0032-5910(83)80002-3.
[23] F. Ayuga, M. Guaita, P.J. Aguado, A. Couto, Discharge and the eccentricity of the hopper influence on the silo wall pressures, J. Eng. Mech. 127 (2001) 1067–1074, https://doi.org/10.1061/(ASCE)0733-9399(2001)127:10(1067).
[24] M. Guaita, A. Couto, F. Ayuga, Numerical simulation of wall pressure during discharge of granular material from cylindrical silos with eccentric hoppers, Biosyst. Eng. 85 (2003) 101–109, https://doi.org/10.1016/S1537-5110(03)00037-0.
[25] P. Vidal, E. Gallego, M. Guaita, F. Ayuga, Simulation of the filling pressures of cylindrical steel silos with concentric and eccentric hoppers using 3-dimensional finite element models, Trans. ASABE 49 (2006) 1881–1895, https://doi.org/10.13031/2013.22290.
[26] P. Vidal, E. Gallego, M. Guaita, F. Ayuga, Finite element analysis under different boundary conditions of the filling of cylindrical steel silos having an eccentric hopper, J. Constr. Steel Res. 64 (2008) 480–492, https://doi.org/10.1016/j.jcsr.2007.08.005.
[27] E. Gallego, J.M. Fuentes, F. Ayuga, A semi-empirical equation to predict filling wall pressures on oblique conical hoppers, Int. Agrophysics 36 (2022) 285–295, https://doi.org/10.31545/intagr/152675.
[28] Y. Wang, F. Jia, J. Zhang, Y. Han, P. Chen, A. Li, J. Fei, W. Feng, X. Hao, S. Shen, Model construction method of discharge rate of eccentric silo, Powder Technol. 405 (2022) 117555, https://doi.org/10.1016/j.powtec.2022.117555.
[29] H. Guo, X. Yang, Z. Tian, T. Li, X. Liu, DEM modeling of the dilute-to-dense transition of granular flow in silos, Powder Technol. 436 (2024) 119472, https://doi.org/10.1016/j.powtec.2024.119472.
[30] M. You, X. Wang, Y. Shi, B. Luo, C. Liang, D. Liu, J. Ma, X. Chen, The dynamic evolution of powder flow and wall normal stress in different flow pattern silos, Int. J. Multiphase Flow 176 (2024) 104844, https://doi.org/10.1016/j.ijmultiphaseflow.2024.104844.
[31] M. Wójcik, M. Sondej, K. Rejowski, J. Tejchman, Full-scale experiments on wheat flow in steel silo composed of corrugated walls and columns, Powder Technol. 311 (2017) 537–555, https://doi.org/10.1016/j.powtec.2017.01.066.
[32] M. Molenda, S.A. Thompson, I.J. Ross, PH—postharvest technology: friction of wheat on corrugated and smooth galvanized steel surfaces, J. Agric. Eng. Res. 77 (2000) 209–219, https://doi.org/10.1006/jaer.2000.0591.
[33] J.M. Fuentes, A. Pinilla, M. Madrid, J. Wiącek, E. Ayuga-Téllez, F. Ayuga, E. Gallego, Measurement of friction phenomena on silo walls made of corrugated steel, Comput. Electron. Agric. 226 (2024) 109374, https://doi.org/10.1016/j.compag.2024.109374.
[34] D.W. Moore, G.M. White, I.J. Ross, Friction of wheat on corrugated metal surfaces, Transact. ASAE 27 (1984) 1842–1847, https://doi.org/10.13031/2013.33055)@1984.
[35] P.A. Versavel, M.G. Britten, Interaction of bulk wheat with bin wall configuration in model bins, Transact. ASAE 29 (2) (1986) 533–537, https://doi.org/10.13031/2013.30186.
[36] M.G. Britton, N.J. Klassen, Wheat friction on steel. Proceedings of international winter meeting American Society of Agricultural Engineers, paper 87-4527, Hyatt regency Chicago in Illinois center, December 15–18, 1987, 1987.
[37] M. Molenda, J. Horabik, I.J. Ross, Loads in model grain bins as affected by filling methods, Transact. ASAE 36 (1993) 915–919, https://doi.org/10.13031/2013.28416.
[38] M. Wójcik, P. Iwicki, J. Tejchman, 3D buckling analysis of a cylindrical metal bin composed of corrugated sheets strengthened by vertical stiffeners, Thin-Walled Struct. 49 (2011) 947–963, https://doi.org/10.1016/j.tws.2011.03.010.
[39] N. Kuczyńska, M. Wójcik, J. Tejchman, Effect of bulk solid on strength of cylindrical corrugated silos during filling, J. Constr. Steel Res. 115 (2015) 1–17, https://doi.org/10.1016/j.jcsr.2015.08.002.
[40] A. Grabowski, M. Nitka, J. Tejchman, Micro-modelling of shear localization during quasi-static confined granular flow in silos using DEM, Comput. Geotech. 134 (2021) 104108, https://doi.org/10.1016/j.compgeo.2021.104108.
[41] M. Nitka, A. Grabowski, Shear band evolution phenomena in direct shear test modelled with DEM, Powder Technol. 391 (2021) 369–384, https://doi.org/10.1016/j.powtec.2021.06.025.
[42] J. Wiącek, P. Parafiniuk, M. Molenda, J. Horabik, E. Gallego, DEM study of microstructural effects in friction of wheat on corrugated steel surface, Tribol. Int. 183 (2023) 108435, https://doi.org/10.1016/j.triboint.2023.108435.
[43] E. Gallego, M. Madrid, J.M. Fuentes, J. Wiącek, A. Grande, F. Ayuga, DEM analysis of friction of cylindrical pinewood pellets with corrugated steel silo walls, Comput. Part. Mech. (2025), https://doi.org/10.1007/s40571-025-00906-3.
[44] J. Tejchman, J. Gorski, Computations of size effects in granular bodies within micro-polar hypoplasticity during plane strain compression, Int. J. Solids Struct. 45 (2008) 1546–1569, https://doi.org/10.1016/j.ijsolstr.2007.10.007.
[45] A. Ruiz, A. Couto, P.J. Aguado, Design and instrumentation of a mid-size test station for measuring static and dynamic pressures in silos under different conditions – part II: construction and validation, Comput. Electron. Agric. 85 (2012) 174–187, https://doi.org/10.1016/j.compag.2012.04.008.
[46] E. Gallego, J.M. Fuentes, Á. Ruiz, G. Hernández-Rodrigo, P. Aguado, F. Ayuga, Determination of mechanical properties for wood pellets used in DEM simulations, International Agrophysics 34 (2020), https://doi.org/10.31545/intagr/130634.
[47] M.A. Madrid, J.M. Fuentes, F. Ayuga, E. Gallego, Determination of the angle of repose and coefficient of rolling friction for wood pellets, Agronomy 12 (2022) 424, https://doi.org/10.3390/agronomy12020424.
[48] M. Moya, D. Sánchez, J.R. Villar-García, Values for the mechanical properties of wheat, maize and wood pellets for use in Silo load calculations involving numerical methods, Agronomy 12 (2022), https://doi.org/10.3390/agronomy12061261.
[49] J.H. Zar, Biostatistical Analysis, Pearson New International, Harlow, England, 2014.
[50] L. Mwinuka, E.O. Hyera, Effect of socio-cultural factors on gendered decision-making in the adoption of improved maize storage technologies, Cogent Food & Agriculture 8 (2022) 2132849, https://doi.org/10.1080/23311932.2022.2132849.
[51] H. Norasi, J. Drum, T. Baldus, G. Mirka, Development of a test battery for fatigue assessment of agriculture seating systems: a laboratory and field study, J. Agromedicine 27 (2022) 346–358, https://doi.org/10.1080/1059924X.2021.2024469.
[52] S.I.E. Perez, Y. Lin, L. Sun, F. Yang, Y. Cai, Microbial community structure, co-occurrence network and fermentation characteristics of woody plant silage, J. Sci. Food Agric. 102 (2022) 1193–1204, https://doi.org/10.1002/jsfa.11457.
[53] A. Nanda, B.B. Mohapatra, Abikesh Prasada Kumar Mahapatra, Abiresh Prasad Kumar Mahapatra, Abinash Prasad Kumar Mahapatra, Multiple comparison test by Tukey's honestly significant difference (HSD): do the confident level control type I error, Int. J. Statist. Appl. Math. 6 (2021) 59–65, https://doi.org/10.22271/maths.2021.v6.i1a.636.
[54] D. Schulze, Powders and Bulk Solids, Springer, Berlin, 2008, https://doi.org/10.1007/978-3-540-73768-1.
[55] E. Gallego, A. Ruiz, P.J. Aguado, Simulation of silo filling and discharge with experimental data, Comput. Electron. Agric. 118 (2015) 281–289, https://doi.org/10.1016/j.compag.2015.09.014.
[56] R.M. Gandia, F.C. Gomes, W.C. de Paula, E.A. de Oliveira Junior, P.J. Aguado Rodriguez, Static and dynamic pressure measurements of maize grain in silos under different conditions, Biosyst. Eng. 209 (2021) 180–199, https://doi.org/10.1016/j.biosystemseng.2021.07.001.
[57] R.M. Gandia, F.C. Gomes, W.C. De Paula, P.J. Aguado Rodriguez, Evaluation of pressures in slender silos varying hopper angle and silo slenderness, Powder Technol. 394 (2021) 478–495, https://doi.org/10.1016/j.powtec.2021.08.087.
[58] D. Zare, A. Nourmohamadi-Moghadami, S.S. Panigrahi, A. Karim, C.B. Singh, Dimensionless modeling of fine material distribution in an experimental silo during central spout loading, J. Stored Prod. Res. 100 (2023) 102063, https://doi.org/10.1016/j.jspr.2022.102063.
[59] A. Drescher, Analytical Methods in Bin-Load Analysis, Developments in Civil Engineering, Elsevier, 1991.
[60] J. Nielsen, Pressures from flowing granular solids in silos, Philosophical Transactions: Mathematical, Physical and Engineering Sciences 356 (1998) 2667–2684, https://doi.org/10.1098/rsta.1998.0292.
[61] Y. Chen, C. Liang, X. Wang, X. Guo, X. Chen, D. Liu, Static pressure distribution characteristics of powders stored in silos, Chem. Eng. Res. Des. 154 (2020) 1–10, https://doi.org/10.1016/j.cherd.2019.10.050.

[62] B. Chen, A. Roberts, T. Donohue, DEM modelling of Silo loads asymmetry induced by eccentric discharge, in: X. Li, Y. Feng, G. Mustoe (Eds.), Presented at the Proceedings of the, Springer Singapore, Singapore, 2017, pp. 1133–1141.
[63] A.W. Jenike, Storage and Flow of Solids, University of North Texas Libraries, UNT Digital Library, United States, 1964.
[64] J. Krzyżanowski, J. Tejchman, M. Wójcik, Modelling of full-scale silo experiments with flow correcting inserts using material point method (MPM) based on hypoplasticity, Powder Technol. 392 (2021) 375–392, https://doi.org/10.1016/j.powtec.2021.06.059.
[65] J. Tejchman, Confined Granular Flow in Silos. Experimental and Numerical Investigations, Springer, 2013, https://doi.org/10.1007/978-3-319-00318-4.
[66] S. Albaraki, S.J. Antony, How does internal angle of hoppers affect granular flow? Experimental studies using digital particle image velocimetry, Powder Technol. 268 (2014) 253–260, https://doi.org/10.1016/j.powtec.2014.08.027.
[67] R. Kobyłka, J. Horabik, M. Molenda, Numerical simulation of the dynamic response due to discharge initiation of the grain silo, Int. J. Solids Struct. 106 (2017) 27–37, https://doi.org/10.1016/j.ijsolstr.2016.12.001.
[68] X. Wang, C. Liang, X. Guo, Y. Chen, D. Liu, J. Ma, X. Chen, H. An, Experimental study on the dynamic characteristics of wall normal stresses during silo discharge, Powder Technol. 363 (2020) 509–518, https://doi.org/10.1016/j.powtec.2020.01.023.
[69] A.W. Jenike, J.R. Johanson, Bins loads, J Struct. Division ASCE 94 (4) (1968) 1011–1041, https://doi.org/10.1061/JSDEAG.0001928.
[70] A.J. Sadowski, J.M. Rotter, J. Nielsen, A theory for pressures in cylindrical silos under concentric mixed flow, Chem. Eng. Sci. 223 (2020) 115748, https://doi.org/10.1016/j.ces.2020.115748.
[71] A. Couto, A. Ruiz, L. Herráez, J. Moran, P.J. Aguado, Measuring pressures in a slender cylindrical silo for storing maize. Filling, static state and discharge with different material flow rates and comparison with Eurocode 1 - part 4, Comput. Electron. Agric. 96 (2013) 40–56, https://doi.org/10.1016/j.compag.2013.04.011.
[72] W.A. Beverloo, H.A. Leniger, J.V. de Velde, The flow of granular solids through orifices, Chem. Eng. Sci. 15 (1961) 260–269, https://doi.org/10.1016/0009-2509(61)85030-6.
[73] P.A. Gago, M.A. Madrid, S. Boettcher, R. Blumenfeld, P. King, Effect of bevelled silo outlet in the flow rate during discharge, Powder Technol. 428 (2023) 118842, https://doi.org/10.1016/j.powtec.2023.118842.
[74] G. Sun, Q. Chen, R. Li, T. Mu, H. Yang, Mass discharge rate of granular flow in eccentric silos with variable side wall friction, Powder Technol. 449 (2025) 120438, https://doi.org/10.1016/j.powtec.2024.120438.
[75] Y. Wang, F. Jia, J. Zhang, Y. Han, P. Chen, A. Li, J. Fei, W. Feng, X. Hao, S. Shen, Model construction method of discharge rate of eccentric silo, Powder Technol. 405 (2022) 117555, https://doi.org/10.1016/j.powtec.2022.117555.

**Adriano Pinilla** is an Agricultural Engineer whose field of expertise is related to rural infrastructures. He is currently pursuing the PhD by conducting the thesis "Experimental analysis of friction in a model silo with corrugated walls" at BIPREE Research Group (Universidad Politecnica de Madrid), and he has already published one paper in a SCI journal and 3 papers in conferences from the works developed in his PhD.

**José María Fuentes Pardo** is an Associate Professor at Universidad Politécnica de Madrid. His current research topics include mechanical properties of granular materials, structural design of silos and numerical methods for structural engineering. Author of 34 publications indexed in Web of Science.

**Francisco Ayuga** Agricultural Engineer PhD, Full Professor at the Polytechnic University of Madrid since 2002. Head of the Agricultural Engineering Department. Specialized in building and rural infrastructures. Coordinator of the Master's Degree in Agricultural Engineering. Vice-president of the Building and Infrastructures Committee of the Spanish Engineering Institute. Former president of the Spanish Society of Agriengineering. Participant in 76 research projects or technological innovation reports for companies. Author of 98 scientific articles and supervisor of 20 doctoral theses. Evaluator of research projects for regional, national and international organisations. Member of the steering committee of 4 international engineering networks.

**Eutiquio Gallego Vázquez** is Associate Professor at BIPREE Research Group (Universidad Politecnica de Madrid). He has published more than 40 papers in journals included in SCI database, most of them related to rural infrastructures (silos, low volume roads or underground cellars). His main field of expertise is the development of numerical models based on Finite Element and Discrete Element techniques for the analysis of problems related to the handling of granular materials in silos.